

Deep Time-series Forecasting Needs Kernelized Moment Balancing

Licheng Pan¹ Hao Wang¹ Haocheng Yang² Yuqi Li³ Qingsong Wen⁴
 Xiaoxi Li¹ Zhichao Chen⁵ Haoxuan Li⁶ Zhixuan Chu⁷ Yuan Lu¹

Abstract

Deep time-series forecasting can be formulated as a distribution balancing problem aimed at aligning the distribution of the forecasts and ground truths. According to Imbens' criterion, true distribution balance requires matching the first moments with respect to any balancing function. We demonstrate that existing objectives fail to meet this criterion, as they enforce moment matching only for one or two predefined balancing functions, thus failing to achieve full distribution balance. To address this limitation, we propose direct forecasting with kernelized moment balancing (KMB-DF). Unlike existing objectives, KMB-DF adaptively selects the most informative balancing functions from a reproducing kernel hilbert space (RKHS) to enforce sufficient distribution balancing. We derive a tractable and differentiable objective that enables efficient estimation from empirical samples and seamless integration into gradient-based training pipelines. Extensive experiments across multiple models and datasets show that KMB-DF consistently improves forecasting accuracy and achieves state-of-the-art performance. Code is available at <https://anonymous.4open.science/r/KMB-DF-403C>.

1. Introduction

Deep time-series forecasting aims to utilize neural networks to predict future values from historical observations, which has been integral to various fields (Benidis et al., 2022; Wang et al., 2024b), such as asset pricing in finance (Li et al., 2025), user visit prediction in e-commerce (Chen et al., 2023), and weather prediction in meteorology (Wu

¹Xiaohongshu Inc. ²National University of Singapore ³The City University of New York, CUNY ⁴Squirrel AI ⁵State Key Lab of General AI, School of Intelligence Science and Technology, Peking University ⁶Center for Data Science, Peking University ⁷College of Computer Science and Technology, Zhejiang University. Correspondence to: Zhixuan Chu <zhixuanchu@zju.edu.cn>, Yuan Lu <luyuan2@xiaohongshu.com>.

et al., 2023b). Currently, the progress in this field primarily revolves around two aspects (Wang et al., 2025a; 2026a): (1) the devise of neural architectures serving as the forecast models, and (2) the design of learning objectives driving model training. Both aspects are essential for improving forecast performance (Qiu et al., 2025).

The devise of neural architectures has been widely studied. The key challenge arises from the input autocorrelation, where different steps in input sequence are correlated. To address this challenge, various architectures have been proposed (Chen et al., 2025; Lin et al., 2025; Wang et al., 2023). A significant advancement lies in Transformer-based models, which employ self-attention mechanisms to model input autocorrelation while scaling effectively to complex tasks (Jin et al., 2024; Lin et al., 2024; Liu et al., 2024b; Nie et al., 2023). Other progresses include recurrent neural networks (Kong et al., 2025), convolutional neural networks (Luo & Wang, 2024), and linear models (Yue et al., 2025; Zeng et al., 2023), each possessing unique inductive biases and strengths in modeling input autocorrelation.

The design of learning objectives has also garnered significant attention (Cuturi & Blondel, 2017; Kudrat et al., 2025; Qiu et al., 2025). The key challenge arises from the label autocorrelation, where different steps in label sequence are correlated, which renders standard objectives like mean squared error (MSE) biased. To accommodate label autocorrelation, Wang et al. (2026b) demonstrated that balancing the distributions of the forecast and label sequences ensures unbiased training of forecast models despite label autocorrelation. However, according to Imbens' criterion (Imbens & Rubin, 2015), if the two distributions are balanced, their first moments should be equivalent with respect to any balancing function. *We demonstrate that existing objectives enforce this equivalence for only one or two predefined functions (Wang et al., 2025a;b; 2026a;b); consequently, they fail to satisfy the criterion and achieve full distribution balancing essential for training forecast models.*

To address the limitation of existing objectives, we propose direct forecasting with kernelized moment balancing (KMB-DF). The core strategy involves adaptively selecting the most informative balancing functions from a reproducing kernel hilbert space (RKHS) associated with univer-

sal kernels. By leveraging the rich capacity of the RKHS, KMB-DF enforces sufficient distribution balancing with theoretical guarantees. Furthermore, we derive a tractable, differentiable objective that allows for efficient estimation from finite time-series samples and integrates seamlessly into gradient-based training pipelines. Experimental results confirm that KMB-DF consistently outperforms existing objectives, enhances the performance of diverse forecast models, and achieves state-of-the-art performance.

Contributions. The contributions in this work can be summarized as follows. **① We identify a critical limitation in existing learning objectives:** they enforce first-moment equivalence only for limited balancing functions, thereby failing to achieve distribution balancing for training forecast models. **② We propose KMB-DF, a framework that enforces distribution balance for training forecast models.** We provide theoretical guarantees for its balancing sufficiency and demonstrate its seamless integration into gradient-based training pipelines. **③ We substantiate the efficacy of KMB-DF through extensive experiments,** demonstrating that it consistently outperforms existing objectives and achieves state-of-the-art performance.

2. Preliminaries

2.1. Problem definition

In this section, we introduce the deep time-series forecast problem. We use uppercase bold letters (*e.g.*, \mathbf{X}) to denote matrices, lowercase bold letters (*e.g.*, \mathbf{x}) to denote vectors, and lowercase normal letters (*e.g.*, x) to denote scalars. A time-series consists of a sequence of chronologically ordered observations, denoted as $\mathbf{S} = \{\mathbf{s}_1, \mathbf{s}_2, \dots, \mathbf{s}_M\} \in \mathbb{R}^{M \times D}$, where M is the total number of observations and D denotes the number of covariates per observation.

At a given time step n , the task definition requires the following components: (1) the *history sequence* $\mathbf{X} = [\mathbf{s}_{m-H+1}, \dots, \mathbf{s}_m] \in \mathbb{R}^{H \times D}$, where H is the history length; (2) the *label sequence* $\mathbf{Y} = [\mathbf{s}_{m+1}, \dots, \mathbf{s}_{m+T}] \in \mathbb{R}^{T \times D}$, where T is the forecast horizon; (3) the *forecast model* g , which is a neural network mapping \mathbf{X} to a forecast sequence $\hat{\mathbf{Y}}$. The task is to train a neural network g by optimizing an appropriate learning objective, such that for any given \mathbf{X} , the forecast $\hat{\mathbf{Y}}$ accurately approximates the ground-truth label sequence (Wang et al., 2025a; 2024b).

2.2. Learning objectives for deep time-series forecasting

The learning objective plays a central role in deep time-series forecast since it drives the training of forecast models. A widespread objective is mean squared error (MSE), mea-

suring the point-wise divergence between \mathbf{Y} and $\hat{\mathbf{Y}}$:

$$\mathcal{E}_{\text{MSE}} = \left\| \mathbf{Y} - \hat{\mathbf{Y}} \right\|_2^2 = \sum_{t=1}^T (\mathbf{y}_t - \hat{\mathbf{y}}_t)^2. \quad (1)$$

While widespread in modern literature (Liu et al., 2024b; Yi et al., 2023; Yue et al., 2025), \mathcal{E}_{MSE} has a critical limitation: it treats future observations as conditionally independent labels (Hounie et al., 2024), while time-series exhibit a label autocorrelation structure, where \mathbf{y}_t is dependent on its predecessors $\mathbf{y}_{}$ (Zeng et al., 2023). \mathcal{E}_{MSE} disregards this label autocorrelation structure and thus being a biased objective. This phenomenon, termed as autocorrelation bias (Wang et al., 2025a), is delineated in Lemma 2.1.

Lemma 2.1 (Autocorrelation bias). *Let $\mathbf{y} \in \mathbb{R}^T$ be a univariate label sequence with conditional covariance $\Sigma \in \mathbb{R}^{T \times T}$. \mathcal{E}_{MSE} in (1) is biased against the likelihood of \mathbf{y} unless Σ is diagonal, i.e., different steps in \mathbf{y} are conditionally decorrelated given \mathbf{X} .*

To accommodate label autocorrelation, alternative learning objectives have been investigated. One prominent line of work focuses on aligning the latent components of \mathbf{Y} and $\hat{\mathbf{Y}}$. Specifically, they employ a mapping function ϕ and adapt point-wise objectives to align $\phi(\hat{\mathbf{y}})$ with $\phi(\mathbf{Y})$. Exemplars include FreDF (Wang et al., 2025b) and Time-o1 (Wang et al., 2025a), which instantiate ϕ as Fourier transform and principal component analysis, respectively. Theoretically, these objectives ensure unbiased training if the components of $\phi(\mathbf{y})$ are conditionally decorrelated (see Lemma 2.1). However, both Fourier transform and principal component analysis ensure only *marginally decorrelation* of the obtained components, not the required *conditional decorrelation*. **Hence, these objectives fail to ensure unbiased training of forecast models.**

Another line of work aims to align the morphological shapes of \mathbf{Y} and $\hat{\mathbf{Y}}$. The premise is that label autocorrelation is reflected in the shape of label sequence; thus, shape dissimilarity measures can serve as autocorrelation-aware objectives. Dynamic time wrapping (Sakoe & Chiba, 2003) (DTW) is a standard shape dissimilarity measure for time-series but suffers from non-differentiability. To address this, SoftDTW (Cuturi & Blondel, 2017) provides a differentiable relaxation, enabling end-to-end training of deep forecast models. Building on this, Dilate (Le Guen & Thome, 2019) combines SoftDTW with a temporal distortion index to penalize lag mismatches, while STRIPE (Le Guen & Thome, 2023) extends these concepts to probabilistic forecasting. **Nonetheless, these objectives remain predominantly heuristic** and lack rigorous theoretical guarantees for unbiasedness in the presence of label autocorrelation. ¹.

¹As a growing literature, there are other learning objectives for

2.3. Distribution balancing and Imbens' criterion

Two distributions are termed *balancing* if they are indistinguishable with respect to all distributional statistics. [Imbens & Rubin \(2015\)](#) introduced a criterion that defines ideal balancing between two distributions \mathbb{P}_1 and \mathbb{P}_2 as:

$$\forall \phi : \mathbb{E}_{z \in \mathbb{P}_1} [\phi(z)] = \mathbb{E}_{z \in \mathbb{P}_2} [\phi(z)], \quad (2)$$

where ϕ is an arbitrary balancing function. This equality is required to hold for any choice of ϕ , which ensures that \mathbb{P}_1 and \mathbb{P}_2 have equivalent first moment under any transformation. This criterion is widely used to assess distribution balancing in diverse fields, such as causal inference ([Fong et al., 2018](#); [Imai & Ratkovic, 2014](#)) and trustworthy machine learning ([Li et al., 2023](#)).

3. Methodology

3.1. Motivation

The training of deep time-series forecast models can be interpreted as a distribution balancing problem ([Wang et al., 2026b](#)). If $\mathbb{P}(\mathbf{Y}|\mathbf{X})$ and $\mathbb{P}(\hat{\mathbf{Y}}|\mathbf{X})$ are balanced, the forecast model is considered accurately trained, as it correctly captures the data-generating process of the label sequence. Likelihood-based objectives like \mathcal{E}_{MSE} pursue this goal by imposing parametric assumptions; specifically, they assume $\mathbb{P}(\mathbf{Y}|\mathbf{X})$ follows a Gaussian distribution with diagonal covariance, which induces autocorrelation bias (see [Lemma 2.1](#)). Subsequent objectives mitigate this by aligning latent components ([Wang et al., 2025a;b; 2026a](#)) or morphological shapes ([Cuturi & Blondel, 2017](#); [Le Guen & Thome, 2019](#)) of \mathbf{Y} and $\hat{\mathbf{Y}}$; however, as discussed in Section 2.2, they are heuristic and lack unbiasedness guarantees.

These findings motivate objectives that enforce distribution balance directly, without resorting to parametric assumptions that introduce autocorrelation bias. Imbens' criterion formalizes the status of distribution balance in (2). Indeed, this criterion has been pursued by existing objectives for specific choices of ϕ . For example, \mathcal{E}_{MSE} seeks to ensure (2) given ϕ is an identity map, and other variants are summarized in Table 1. However, Imbens' criterion requires (2) to hold for **all** ϕ , whereas current objectives enforce it for only **one or two specified** balancing functions. As a result, they do not generally satisfy Imbens' criterion and fail to achieve true distribution balance for training forecast models.

Given the potential of distribution balancing and the failure of existing objectives to achieve it, it is essential to investigate objectives that directly target distribution balancing as

training deep forecast models ([Kudrat et al., 2025](#); [Qiu et al., 2025](#); [Wang et al., 2024a](#); [Wu et al., 2020](#); [Xiong et al., 2025](#)). While they often improve upon \mathcal{E}_{MSE} , they are not explicitly designed to accommodate label autocorrelation central to this paper. Thus, we list them for completeness but omit further discussion for brevity.

Table 1. The choice of ϕ in recent learning objectives for deep time-series forecast ([Wang et al., 2025a;b; 2026a;b](#)).

| Method | Year | Choice of ϕ | Number of ϕ |
|---------|------|-------------------------------|------------------|
| FreDF | 2025 | Discrete Fourier transform. | 1 |
| Time-o1 | 2025 | Principal component analysis. | 1 |
| QDF | 2025 | Meta-learned linear mapping. | 1 |
| DistDF | 2025 | Mean and variance statistics. | 2 |

defined by Imbens' criterion. Critically, three research questions warrant investigation: (1) *How to formulate learning objective based on Imbens' criterion for training forecast models?* (2) *Do they come with theoretical guarantees?* (3) *Do they improve forecast performance in practice?*

3.2. Distribution balancing with specified ϕ

In this section, we develop a distribution balancing strategy to train forecast models. Notably, directly balancing the conditional distributions $\mathbb{P}(\mathbf{Y}|\mathbf{X})$ and $\mathbb{P}(\hat{\mathbf{Y}}|\mathbf{X})$ is intractable given finite-sample time-series datasets². Inspired by [Wang et al. \(2026b\)](#), we instead balance the joint distributions $\mathbb{P}(\mathbf{Y}, \mathbf{X})$ and $\mathbb{P}(\hat{\mathbf{Y}}, \mathbf{X})$, which is effective for two reasons: (i) $\mathbb{P}(\mathbf{Y}, \mathbf{X}) = \mathbb{P}(\hat{\mathbf{Y}}, \mathbf{X})$ implies $\mathbb{P}(\mathbf{Y}|\mathbf{X}) = \mathbb{P}(\hat{\mathbf{Y}}|\mathbf{X})$ for all \mathbf{X} , thus ensuring effective training of forecast models; (ii) joint balancing is tractable since all samples in the dataset can be used to estimate and balance the joint distributions.

Let $\mathbf{Z} = (\mathbf{Y}, \mathbf{X})$ and $\hat{\mathbf{Z}} = (\hat{\mathbf{Y}}, \mathbf{X})$ denote the joint random variables. According to Imbens' criterion (2), the two joint distributions are balanced if we have

$$\forall \phi : \mathbb{E}_{\mathbf{Z} \in \mathbb{P}(\mathbf{Z})} [\phi(\mathbf{Z})] = \mathbb{E}_{\hat{\mathbf{Z}} \in \mathbb{P}(\hat{\mathbf{Z}})} [\phi(\mathbf{Z})], \quad (3)$$

Given a finite time-series samples $\mathbf{Z}^{(n)} = (\mathbf{X}^{(n)}, \mathbf{Y}^{(n)})$ and forecasts $\hat{\mathbf{Z}}^{(n)} = (\mathbf{X}^{(n)}, \hat{\mathbf{Y}}^{(n)})$ with $n = 1, \dots, N$ and $\hat{\mathbf{Y}}^{(n)} = g_{\theta}(\mathbf{X}^{(n)})$; one can attempt to enforce (3) over a chosen set of balancing functions $\{\phi_k\}_{k=1}^K$. This yields the constrained learning problem as follow:

$$\begin{aligned} \min_{\theta} \sum_{n=1}^N & \left\| \mathbf{Y}^{(n)} - \hat{\mathbf{Y}}^{(n)} \right\|_2^2 \\ \text{s.t. } & \sum_{n=1}^N \phi_k(\mathbf{Z}^{(n)}) = \sum_{n=1}^N \phi_k(\hat{\mathbf{Z}}^{(n)}), \forall k \in [K] \end{aligned} \quad (4)$$

where each constraint enforces balance with respect to certain balancing function ϕ_k . In contrast to the objectives in Table 1, the formulation in (4) increases the number of balancing functions to K . As K grows, the constraints in

²Specifically, for any fixed \mathbf{X} , the dataset contains only one associated label sequence, and the model produces only one forecast sequence. Thus, only one sample can be observed from each of $\mathbb{P}(\mathbf{Y}|\mathbf{X})$ and $\mathbb{P}(\hat{\mathbf{Y}}|\mathbf{X})$, which is insufficient to characterize—and therefore balance—these conditional distributions.

(4) increasingly guarantee the Imbens' criterion, thereby promoting distribution balance between $\mathbb{P}(\mathbf{Z})$ and $\mathbb{P}(\hat{\mathbf{Z}})$.

However, the formulation (4) relies on a predefined set of balancing functions $\{\phi\}_{k=1}^K$. In practice, selecting a finite set of balancing functions that sufficiently depicts distribution discrepancies is difficult. To guarantee (3), one would need to specify infinitely many balancing constraints, rendering (4) computationally intractable. Therefore, it is essential to develop tractable relaxations that selectively enforce balance over the most informative balancing functions.

3.3. Kernel functions, universal property, and kernelized soft-margin balancing

To overcome the reliance on a predefined finite set of balancing functions, we leverage reproducing kernel Hilbert space (RKHS) theory to construct a rich, data-adaptive set of balancing functions and derive a tractable learning problem. We start by clarifying key properties of kernel functions in Definition 3.1 and 3.2.

Definition 3.1 (Kernel function). Let \mathcal{Z} be a non-empty set. A function $K : \mathcal{Z} \times \mathcal{Z} \rightarrow \mathbb{R}$ is a kernel function if there exists a Hilbert space \mathcal{H} and a feature map $\psi : \mathcal{Z} \rightarrow \mathcal{H}$ such that $\forall \mathbf{Z}, \mathbf{Z}' \in \mathcal{Z}, K(\mathbf{Z}, \mathbf{Z}') := \langle \psi(\mathbf{Z}), \psi(\mathbf{Z}') \rangle_{\mathcal{H}}$.

Definition 3.2 (Universal kernel). For \mathcal{Z} a compact Hausdorff space, a universal kernel ensures that any continuous function $e : \mathcal{Z} \rightarrow \mathbb{R}$ can be approximated arbitrarily well within its RKHS. Specifically, for any $\epsilon > 0$, there exists $f \in \mathcal{H}$ such that: $\sup_{\mathbf{Z} \in \mathcal{Z}} |f(\mathbf{Z}) - e(\mathbf{Z})| \leq \epsilon$.

The exponential kernel is a kernel function defined as:

$$K(\mathbf{Z}, \mathbf{Z}') = \exp(-\|\mathbf{Z} - \mathbf{Z}'\|/2\sigma^2),$$

which is a universal kernel defined in Definition 3.2. It implies that functions in the RKHS of K , defined as $\mathcal{H} = \text{span}\{K(\cdot, \mathbf{Z}) \mid \mathbf{Z} \in \mathcal{Z}\}$, can approximate any continuous balancing function. Motivated by this property, it is natural to instantiate the balancing functions as exponential kernel functions anchored by $\{\mathbf{Z}^{(k)}\}_{k=1}^K$:

$$\phi_k(\cdot) = K(\cdot, \mathbf{Z}^{(k)}), \quad \text{i.e., } \forall \mathbf{Z}, \phi_k(\mathbf{Z}) = K(\mathbf{Z}, \mathbf{Z}^{(k)}),$$

which yields K balancing functions.

On this basis, substituting $\phi_k(\cdot) = K(\cdot, \mathbf{Z}^{(k)})$ into (4) yields the following kernelized constraints that are directly computable from the data:

$$\begin{aligned} & \min_{\theta} \sum_{n=1}^N \left\| \mathbf{Y}^{(n)} - \hat{\mathbf{Y}}^{(n)} \right\|_2^2 \\ & \text{s.t. } \sum_{n=1}^N K(\mathbf{Z}^{(n)}, \mathbf{Z}^{(k)}) = \sum_{n=1}^N K(\hat{\mathbf{Z}}^{(n)}, \hat{\mathbf{Z}}^{(k)}), \end{aligned} \quad (5)$$

where $k = 1, 2, \dots, K$. One could directly set $K = N$, i.e., using balancing functions anchored at all samples. However, this introduces N constraints, which is computationally prohibitive and can render the problem over-constrained for large time-series datasets. To obtain a tractable formulation, two refinements to (5) are introduced as follows.

- First, we introduce a selective balancing mechanism. Recognizing that different balancing functions have different abilities to detect imbalance, we quantify the informativeness score of the k -th balancing function as:

$$\delta_k = \sum_{n=1}^N K(\mathbf{Z}^{(n)}, \mathbf{Z}^{(k)}) - \sum_{n=1}^N K(\hat{\mathbf{Z}}^{(n)}, \mathbf{Z}^{(k)}), \quad (6)$$

where $k = 1, 2, \dots, N$; larger $|\delta_k|$ signifies greater detected imbalance. We select only K ($K < N$) balancing functions with the largest $|\delta_k|$ values, and denote their associated anchor samples as $\mathbf{Z}^{(n_1)}, \mathbf{Z}^{(n_2)}, \dots, \mathbf{Z}^{(n_K)}$. By prioritizing the most informative balancing functions, we reduce the number of constraints while maintaining effective distribution balance. This strategy is theoretically grounded in Theorem 3.3, which guarantees distribution alignment between $\mathbb{P}(\mathbf{Z})$ and $\mathbb{P}(\hat{\mathbf{Z}})$ provided that the optimal discrimination function lies within the linear span of the selected balancing functions $\{K(\cdot, \mathbf{Z}^{(n_k)})\}_{k=1}^K$.

- Second, we introduce a soft-margin relaxation mechanism. Since the equality constraints in (5) might be overly rigid—particularly for time-series data, where outliers or abrupt shocks may induce large but spurious imbalances—we replace each equality constraint with a pair of inequality constraints that allow bounded violations, and penalize these violations in the objective.

Theorem 3.3. Suppose \mathcal{H} is the RKHS of a exponential kernel K , $f^* \in \mathcal{H}$ is the discrimination function that maximizes the discrepancy between two distributions \mathbb{P} and \mathbb{Q} . If f^* lies within the linear span of a finite kernel function set: $f^* \in \{K(\cdot, \mathbf{Z}_k)\}_{k=1}^K$; then \mathbb{P} and \mathbb{Q} are balanced if $\forall k \in [K] : \mathbb{E}_{\mathbf{Z} \in \mathbb{P}}[K(\mathbf{Z}, \mathbf{Z}_k)] = \mathbb{E}_{\hat{\mathbf{Z}} \in \mathbb{Q}}[K(\hat{\mathbf{Z}}, \mathbf{Z}_k)]$.

Proof. The proof can be found in Appendix B. \square

The two efforts collectively yield the kernelized soft-margin balancing problem:

$$\begin{aligned} & \min_{\theta} \sum_{n=1}^N \left\| \mathbf{Y}^{(n)} - \hat{\mathbf{Y}}^{(n)} \right\|_2^2 + \kappa \sum_{k=1}^K \varepsilon_k, \quad \varepsilon_k \geq 0, \quad \forall k \in [K] \\ & \text{s.t. } \sum_{n=1}^N K(\mathbf{Z}^{(n)}, \mathbf{Z}^{(n_k)}) - \sum_{n=1}^N K(\mathbf{Z}^{(n)}, \hat{\mathbf{Z}}^{(n_k)}) \leq C + \varepsilon_k, \\ & \quad \sum_{n=1}^N K(\mathbf{Z}^{(n)}, \mathbf{Z}^{(n_k)}) - \sum_{n=1}^N K(\mathbf{Z}^{(n)}, \hat{\mathbf{Z}}^{(n_k)}) \geq -C - \varepsilon_k, \end{aligned} \quad (7)$$

Algorithm 1 The workflow of KMB-DF.

Input: $\mathbf{X}^{(n)}$: history sequences, $\mathbf{Y}^{(n)}$: label sequences.

Parameter: α : the strength of penalty, K : the number of balancing functions, C : the tolerated imbalance, g_θ : the forecast model with parameters θ .

Output: $\mathcal{L}_{\text{KMB-DF}}$: the obtained learning objective.

```

1:  $\hat{\mathbf{Y}}^{(n)} \leftarrow g_\theta(\mathbf{X}^{(n)})$ ,  $n = 1, \dots, N$ 
2:  $\mathbf{Z}^{(n)} = \text{concat}(\mathbf{X}^{(n)}, \mathbf{Y}^{(n)})$ ,  $n = 1, \dots, N$ 
3:  $\hat{\mathbf{Z}}^{(n)} = \text{concat}(\mathbf{X}^{(n)}, \hat{\mathbf{Y}}^{(n)})$ ,  $n = 1, \dots, N$ 
4:  $\delta_k = \sum_{n=1}^N K(\mathbf{Z}^{(n)}, \mathbf{Z}^{(k)}) - K(\mathbf{Z}^{(n)}, \hat{\mathbf{Z}}^{(k)})$ ,  $k = 1, \dots, N$ 
5:  $n_1, \dots, n_K \leftarrow \arg \text{TopK}_n \delta_n$ 
6:  $\xi_{n_k} = [-C - \delta_{n_k}]_+ + [\delta_{n_k} + C]_+$ ,  $k = 1, \dots, K$ 
7:  $\mathcal{E}_{\text{KMB-DF}} \leftarrow \alpha \sum_{k=1}^K \xi_{n_k} + (1 - \alpha) \sum_{n=1}^N \|\mathbf{Y}^{(n)} - \hat{\mathbf{Y}}^{(n)}\|_2^2$ 

```

where $C \geq 0$ controls the tolerated imbalance, $\kappa > 0$ penalizes violations, and ε_k are slack variables. This formulation retains the distribution balancing rationale following Imbens' criterion while becoming computationally tractable for large-scale time-series data.

3.4. Model implementation

In this section, we introduce the implementation of KMB-DF, which adapts the kernelized soft-margin balancing problem to train a deep forecast model g_θ . The main procedure is summarized in Algorithm 1.

Given a set of N samples, each consisting of a history sequence $\mathbf{X}^{(n)}$ and its corresponding label sequence $\mathbf{Y}^{(n)}$, the forecast model generates the forecast sequence (step 1). To perform joint distribution balancing, we construct the extended sequences, where $\text{concat}(\cdot, \cdot)$ denotes concatenation along the time dimension (steps 2-3). Then, we compute informativeness scores for all balancing functions and retain the top K functions with the largest $|\delta_k|$ values (steps 4-5). The final learning objective is defined as follows:

$$\mathcal{E}_{\text{KMB-DF}} = \alpha \sum_{k=1}^K \xi_{n_k} + (1 - \alpha) \sum_{n=1}^N \|\mathbf{Y}^{(n)} - \hat{\mathbf{Y}}^{(n)}\|_2^2$$

where $\xi_{n_k} = [-C - \delta_{n_k}]_+ + [\delta_{n_k} + C]_+$,

$$\delta_{n_k} = \sum_{n=1}^N K(\mathbf{Z}^{(n)}, \mathbf{Z}^{(n_k)}) - \sum_{n=1}^N K(\mathbf{Z}^{(n)}, \hat{\mathbf{Z}}^{(n_k)}), \quad (8)$$

where $[\cdot]_+ = \max(\cdot, 0)$, $0 \leq \alpha \leq 1$ controls the strength of penalty for violating balancing constraints, C controls the margin within which imbalance is tolerated. This unconstrained objective is directly obtained from (7) by introducing the hinge penalties ξ_k , which enables optimization with gradient-based methods (step 7).

By iteratively minimizing $\mathcal{E}_{\text{KMB-DF}}$, KMB-DF improves forecast performance by effectively balancing joint distri-

butions while preserving the benefits of the canonical DF framework (Zeng et al., 2023), such as efficient multi-task training and inference. Moreover, as a model-agnostic learning objective, KMB-DF can be integrated into various forecast models to improve performance.

4. Experiments

To demonstrate the utility of KMB-DF to train forecast models, there are five aspects deserving empirical investigation:

- 1. Performance:** *Does KMB-DF perform well?* In Section 4.2, we compare KMB-DF with previously developed learning objectives for training forecast models.
- 2. Gain:** *Why does it work?* In section 4.3, we perform an ablative study, dissecting the individual components and clarifying their contributions to forecast accuracy.
- 3. Generality:** *Does it support other models and kernels?* In Section 4.4, we analyze the impact of kernel selection, and in Section 4.5, we examine its compatibility with various models, with further results in Appendix D.3.
- 4. Sensitivity:** *Is it sensitive to hyperparameters?* In Section 4.6, we analyze the sensitivity of KMB-DF to the hyperparameter α , K and C , showing stable performance across a broad parameter range.
- 5. Efficiency:** *Is it computationally efficient?* In Appendix D.6, we evaluate the running cost of KMB-DF across different scenarios.

4.1. Setup

Datasets. We evaluate our methods using several standard public benchmarks for long-term time-series forecasting, following Wu et al. (2023a). Specifically, we use the ETT (four subsets), ECL, and Weather (Liu et al., 2024b) datasets. Additionally, we introduce M5 dataset (Makridakis et al., 2022), which is notably challenging. All datasets are split chronologically into training, validation, and test sets. Comprehensive dataset statistics are presented in Appendix C.1.

Baselines. Since this paper focuses on the devise of learning objectives, we select competitive learning objectives tailored for training forecast models as baselines: ① **shape-alignment objectives:** GDTW (Liu et al., 2021), Dilate (Le Guen & Thome, 2019), and Soft-DTW (Cuturi & Blondel, 2017); ② **likelihood maximation objectives:** QDF (Wang et al., 2026a), Time-o1 (Wang et al., 2025a), Koopman (Lange et al., 2021), FreDF (Wang et al., 2025b), and MSE; ③ **distribution balancing objectives:** DistDF (Wang et al., 2026b). The implementation of baselines follows the official codebase from Wang et al. (2026b).

Implementation. We employ CFPT (Kou et al., 2025) as the default forecast model in comparing learning objectives. To ensure fair comparison, the drop-last trick is disabled for all baselines, as recommended in Qiu et al. (2024). All objectives are trained with the Adam optimizer (Kingma & Ba, 2015). When integrating KMB-DF to train a forecast model, we retain all hyperparameters from the public benchmarks (Kou et al., 2025), only tuning α , the learning rate, the tolerated imbalance C and the number of balancing functions K . Experiments are run on Intel(R) Xeon(R) Platinum 8463B CPUs with 32 NVIDIA RTX H800 GPUs. Further implementation details are provided in Appendix C.

4.2. Overall performance

Table 2 presents a comprehensive comparison between KMB-DF and competitive learning objectives. We have the following observations: ① **Shape-alignment objectives suffer from heuristic definitions.** Methods like GDTW, Dilate, and Soft-DTW rely on geometric matching lacking statistical guarantees. Consequently, they yield high variance in performance, particularly failing on complex datasets like ECL where statistical properties dominate geometric shape. ② **Likelihood objectives are limited by autocorrelation bias.** While QDF, Time-o1, and FreDF transform labels to mitigate autocorrelation bias, they achieve only marginal decorrelation. As noted in Section 3.1, they fail to ensure the conditional independence required for unbiased estimation, resulting in limited gains over MSE. ③ **Finite moment balancing fails to satisfy Imbens' criterion.** DistDF aligns distributions using only a few predefined statistics. By neglecting the requirement for moment equivalence across any balancing function, it leaves higher-order distributional discrepancies unaddressed, limiting its effectiveness. ④ **KMB-DF achieves state-of-the-art accuracy through sufficient distribution balancing.** By leveraging the RKHS of universal kernels, KMB-DF effectively enforces Imbens' criterion across an infinite-dimensional space. This allows it to adaptively minimize complex distributional discrepancies, consistently yielding the lowest prediction errors.

Showcases. Figure 1 visualizes forecast snapshots on ETTm1 and ETTh2 datasets with a lookback window of $H = 96$. In the ETTm1 case, the baseline fails to capture the sharp drop at step $n \approx 100$, exhibiting a tendency to revert to the mean. KMB-DF accurately tracks this large-scale shift by enforcing sufficient distribution balance in the RKHS, effectively mitigating the autocorrelation bias that limits point-wise objectives. In the ETTh2 case, the baseline over-smooths high-frequency fluctuations, dampening peaks and troughs. KMB-DF preserves these fine-grained dynamics, as the universal kernels capture the higher-order moments necessary to model complex, non-smooth patterns.

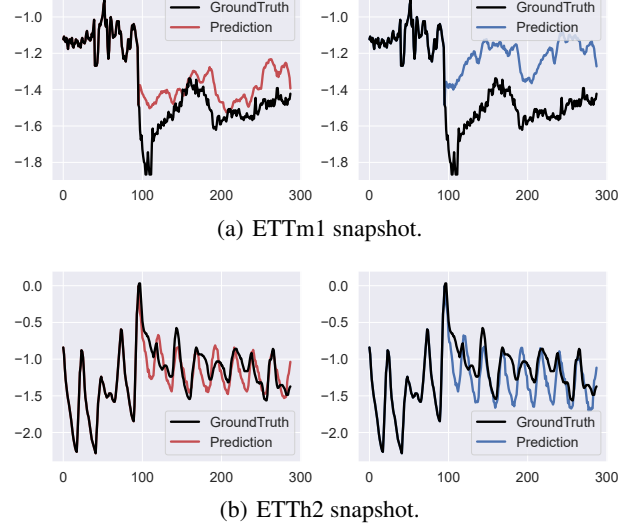


Figure 1. The forecast sequence of MSE (in blue) and KMB-DF (in red), with historical length $H = 96$.

4.3. Ablation studies

In this section, we dissect the contributions of the soft-margin relaxation and the selective balancing mechanism inherent in KMB-DF. Table 3 examines the performance of variants by selectively enabling these components. The main findings are as follows: ① **Soft-margin relaxation tolerates empirical noise.** KMB-DF † incorporates the slack variables in Eq. (7) without selection. It generally outperforms DF, indicating that enforcing strict moment equivalence is overly rigid for time-series data. The soft-margin mechanism effectively accommodates inherent outliers, preventing the kernelized balancing from overfitting to spurious discrepancies. ② **Selective mechanism highlights discriminative kernels.** KMB-DF ‡ employs the informativeness score in Eq. (6) to select balancing functions while maintaining strict constraints. This approach yields improvements by prioritizing the most significant distributional mismatches in the RKHS, thereby avoiding optimization dilution caused by redundant or uninformative balancing constraints. ③ **KMB-DF integrates both for optimal alignment.** The full framework combines flexible soft-margin constraints with informative kernel selection to yield the best performance. This demonstrates a synergistic effect: achieving sufficient distribution balance requires both identifying the most discriminative kernels to align and allowing bounded violations to handle finite-sample noise effectively.

4.4. Kernel function selection studies

In this section, we evaluate the impact of the kernel function choice $K(\cdot, \cdot)$ in instantiating the balancing constraints. We compare the proposed exponential kernel against Linear, Polynomial, Sigmoid, and Gaussian kernels, as detailed in

Deep Time-series Forecasting Needs Kernelized Moment Balancing

Table 2. Comparative results with other objectives for time-series forecasting.

| Loss | KMB-DF | | QDF | | DistDF | | Time-01 | | FreDF | | Koopman | | GDTW | | Dilate | | Soft-DTW | | MSE | |
|---------|--------------|--------------|--------------|--------------|--------------|-------|--------------|--------------|--------------|--------------|---------|-------|-------|-------|--------|-------|----------|-------|-------|-------|
| Metrics | MSE | MAE | MSE | MAE | MSE | MAE | MSE | MAE | MSE | MAE | MSE | MAE | MSE | MAE | MSE | MAE | MSE | MAE | MSE | MAE |
| ETTm1 | 0.372 | 0.391 | <u>0.375</u> | 0.393 | 0.375 | 0.393 | 0.378 | 0.393 | 0.376 | <u>0.392</u> | 0.378 | 0.395 | 0.398 | 0.412 | 0.379 | 0.396 | 0.394 | 0.403 | 0.378 | 0.394 |
| ETTm2 | 0.267 | 0.315 | <u>0.268</u> | 0.315 | 0.269 | 0.315 | 0.271 | <u>0.314</u> | 0.271 | 0.313 | 0.274 | 0.319 | 0.289 | 0.332 | 0.273 | 0.317 | 0.291 | 0.330 | 0.271 | 0.317 |
| ETTh1 | 0.426 | 0.426 | 0.434 | 0.429 | 0.434 | 0.428 | <u>0.430</u> | 0.429 | 0.434 | <u>0.428</u> | 0.437 | 0.431 | 0.452 | 0.444 | 0.441 | 0.434 | 0.461 | 0.445 | 0.436 | 0.430 |
| ETTh2 | 0.364 | 0.394 | 0.367 | 0.396 | <u>0.365</u> | 0.395 | 0.367 | <u>0.394</u> | 0.368 | 0.394 | 0.368 | 0.397 | 0.386 | 0.409 | 0.371 | 0.398 | 0.393 | 0.409 | 0.372 | 0.398 |
| ECL | 0.163 | <u>0.258</u> | <u>0.164</u> | 0.259 | 0.164 | 0.259 | 0.165 | 0.259 | 0.166 | 0.258 | 0.165 | 0.260 | 0.261 | 0.755 | 0.165 | 0.260 | 0.261 | 0.165 | 0.260 | 0.260 |
| Weather | 0.239 | 0.265 | 0.241 | 0.267 | 0.241 | 0.268 | 0.240 | 0.266 | <u>0.240</u> | <u>0.265</u> | 0.246 | 0.272 | 0.248 | 0.276 | 0.246 | 0.273 | 0.262 | 0.281 | 0.241 | 0.267 |
| M5 | 0.152 | 0.309 | 0.156 | <u>0.313</u> | <u>0.156</u> | 0.313 | 0.161 | 0.319 | 0.168 | 0.327 | 0.158 | 0.317 | 0.160 | 0.318 | 0.159 | 0.317 | 0.162 | 0.322 | 0.168 | 0.327 |

Note: We fix the input length as 96 following (Liu et al., 2024b). **Bold** and underlined denote best and second-best results, respectively. Avg indicates average results over forecast horizons: T=96, 192, 336 and 720. TransDF employs the top-performing baseline on each dataset as its underlying forecasting model.

Table 3. Ablation study results.

| Model | Soft-Margin | Selective | Data | T=96 | | T=192 | | T=336 | | T=720 | | Avg | | |
|---------------------|-------------|-----------|---------|--------------|--------------|--------------|--------------|--------------|--------------|--------------|--------------|--------------|--------------|-------|
| | | | | MSE | MAE | |
| DF | X | X | ETTm1 | 0.321 | 0.358 | 0.357 | 0.382 | 0.387 | 0.401 | 0.446 | 0.435 | 0.378 | 0.394 | |
| | | | ETTh1 | 0.373 | 0.391 | 0.427 | 0.421 | 0.466 | 0.441 | 0.477 | 0.468 | 0.436 | 0.430 | |
| | | | ECL | <u>0.137</u> | 0.232 | 0.153 | 0.247 | 0.168 | 0.266 | <u>0.199</u> | <u>0.294</u> | <u>0.165</u> | 0.260 | 0.260 |
| | | | Weather | 0.156 | 0.201 | 0.205 | 0.245 | 0.261 | 0.286 | 0.343 | 0.339 | 0.241 | 0.267 | 0.267 |
| KMB-DF [†] | ✓ | X | ETTm1 | <u>0.318</u> | <u>0.356</u> | <u>0.355</u> | 0.381 | <u>0.383</u> | <u>0.400</u> | <u>0.442</u> | <u>0.433</u> | <u>0.374</u> | <u>0.392</u> | |
| | | | ETTh1 | 0.372 | 0.391 | <u>0.423</u> | 0.421 | 0.462 | <u>0.443</u> | 0.462 | 0.469 | 0.430 | 0.431 | |
| | | | ECL | 0.137 | <u>0.232</u> | <u>0.153</u> | <u>0.247</u> | <u>0.168</u> | <u>0.265</u> | 0.201 | 0.294 | 0.165 | <u>0.259</u> | |
| | | | Weather | 0.154 | 0.199 | <u>0.204</u> | <u>0.242</u> | 0.261 | 0.286 | 0.342 | 0.341 | 0.240 | 0.267 | |
| KMB-DF [‡] | X | ✓ | ETTm1 | 0.318 | 0.356 | 0.356 | <u>0.380</u> | 0.384 | 0.401 | 0.442 | <u>0.433</u> | 0.375 | 0.393 | |
| | | | ETTh1 | 0.372 | 0.389 | 0.425 | 0.420 | 0.458 | <u>0.439</u> | <u>0.455</u> | <u>0.457</u> | <u>0.427</u> | <u>0.426</u> | |
| | | | ECL | 0.137 | 0.232 | 0.153 | 0.247 | 0.168 | 0.266 | 0.200 | 0.294 | 0.165 | 0.260 | |
| | | | Weather | <u>0.153</u> | <u>0.198</u> | 0.205 | 0.244 | <u>0.261</u> | <u>0.285</u> | <u>0.341</u> | <u>0.338</u> | <u>0.240</u> | <u>0.266</u> | |
| KMB-DF | ✓ | ✓ | ETTm1 | 0.313 | 0.354 | <u>0.351</u> | 0.379 | <u>0.381</u> | 0.400 | 0.442 | 0.433 | 0.372 | 0.391 | |
| | | | ETTh1 | <u>0.372</u> | <u>0.389</u> | <u>0.423</u> | <u>0.421</u> | <u>0.460</u> | <u>0.438</u> | <u>0.447</u> | <u>0.455</u> | <u>0.426</u> | <u>0.426</u> | |
| | | | ECL | 0.136 | 0.231 | <u>0.152</u> | <u>0.245</u> | <u>0.168</u> | <u>0.265</u> | <u>0.198</u> | <u>0.293</u> | <u>0.163</u> | <u>0.258</u> | |
| | | | Weather | 0.152 | 0.196 | 0.204 | <u>0.242</u> | <u>0.260</u> | <u>0.284</u> | <u>0.339</u> | <u>0.337</u> | <u>0.239</u> | <u>0.265</u> | |

Note: **Bold** and underlined denote best and second-best results, respectively.

Table 4. Varying kernel function results.

| Kernel | ETTh1 | | | | ETTm1 | | | |
|-------------|-------|--------------|-------|--------------|-------|--------------|-------|--------------|
| | MSE | ΔMSE | MAE | ΔMAE | MSE | ΔMSE | MAE | ΔMAE |
| DF | 0.436 | - | 0.430 | - | 0.378 | - | 0.394 | - |
| Linear | 0.435 | <u>0.3%↓</u> | 0.428 | <u>0.4%↓</u> | 0.375 | <u>0.7%↓</u> | 0.393 | <u>0.3%↓</u> |
| Polynomial | 0.434 | <u>0.4%↓</u> | 0.430 | <u>0.1%↓</u> | 0.375 | <u>0.7%↓</u> | 0.393 | <u>0.3%↓</u> |
| Sigmoid | 0.433 | <u>0.6%↓</u> | 0.430 | <u>0.0%↑</u> | 0.375 | <u>0.9%↓</u> | 0.392 | <u>0.5%↓</u> |
| Gaussian | 0.434 | <u>0.5%↓</u> | 0.430 | <u>0.1%↓</u> | 0.374 | <u>1.0%↓</u> | 0.392 | <u>0.4%↓</u> |
| Exponential | 0.426 | <u>2.3%↓</u> | 0.426 | <u>1.1%↓</u> | 0.372 | <u>1.6%↓</u> | 0.391 | <u>0.7%↓</u> |

Table 4. Two key observations are derived: **1 Kernelized balancing provides effective regularization.** All kernel-based objectives consistently outperform DF. This confirms that incorporating moment balancing constraints provides a necessary supervision signal that complements the pointwise MSE loss, thereby mitigating the overfitting to biased likelihoods associated with label autocorrelation. **2 Universal kernels ensure sufficient distribution balancing.** Universal kernels (Exponential and Gaussian) outperform non-universal ones, validating our theoretical motivation. Unlike non-universal kernels that enforce matching only up to a finite order, universal kernels map representations into an infinite-dimensional RKHS. This capacity enables KMB-DF to satisfy Imbens' criterion by capturing the high-order moments required for sufficient alignment, with the exponential kernel yielding the most significant gains.

Table 5. Varying α results.

| α | ETTh1 | | | | ETTm1 | | | |
|----------|-------|--------------|-------|--------------|-------|--------------|-------|--------------|
| | MSE | ΔMSE | MAE | ΔMAE | MSE | ΔMSE | MAE | ΔMAE |
| DF | 0.436 | - | 0.430 | - | 0.378 | - | 0.394 | - |
| 0.1 | 0.433 | <u>0.8%↓</u> | 0.428 | <u>0.5%↓</u> | 0.374 | <u>1.0%↓</u> | 0.392 | <u>0.4%↓</u> |
| 0.3 | 0.431 | <u>1.1%↓</u> | 0.428 | <u>0.4%↓</u> | 0.373 | <u>1.2%↓</u> | 0.393 | <u>0.2%↓</u> |
| 0.5 | 0.433 | <u>0.7%↓</u> | 0.430 | <u>0.1%↓</u> | 0.374 | <u>1.1%↓</u> | 0.392 | <u>0.5%↓</u> |
| 0.7 | 0.426 | <u>2.3%↓</u> | 0.426 | <u>0.9%↓</u> | 0.374 | <u>1.1%↓</u> | 0.392 | <u>0.5%↓</u> |
| 0.9 | 0.431 | <u>1.1%↓</u> | 0.429 | <u>0.3%↓</u> | 0.373 | <u>1.3%↓</u> | 0.392 | <u>0.6%↓</u> |

4.5. Generalization Studies

In this section, we assess the generalizability of KMB-DF by integrating it into four representative state-of-the-art forecast models: CFPT (Kou et al., 2025), TimeBridge (Liu et al., 2024a), Fredformer (Piao et al., 2024), and iTransformer (Liu et al., 2024b). The performance improvements are visualized in Figure 2. We observe consistent performance boosts across these diverse architectures, highlighted by substantial error reductions, such as an 8.2% drop in MSE for Fredformer on the ECL dataset. These results demonstrate that KMB-DF functions as a broadly compatible, model-agnostic learning objective. By enforcing strict distribution balance via kernelized moment matching, KMB-DF effectively corrects the distributional misalignment that standard objectives fail to address, thereby unlocking the latent predictive potential of existing models.

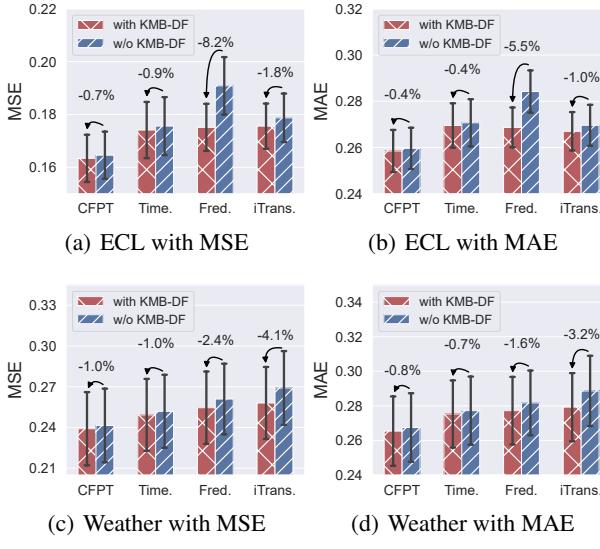


Figure 2. Improvement of KMB-DF applied to different forecast models, shown with colored bars for means over forecast lengths (96, 192, 336, 720) and error bars for 50% confidence intervals.

4.6. Hyperparameter sensitivity

In this section, we examine the impact of key hyperparameters on KMB-DF’s performance, including the penalty strength α , the tolerated imbalance margin C , and the number of balancing functions K . The experimental results are reported in Tables 5, 6, and 7. The primary observations are summarized as follows:

- The coefficient α governs the trade-off between the standard MSE loss and the kernelized moment balancing penalty. As shown in Table 5, increasing α from 0.1 generally yields performance gains, identifying an optimal range around $\alpha \in [0.3, 0.7]$. Specifically, on the ETTh1 dataset, $\alpha = 0.7$ achieves the lowest MSE, reducing it by 2.3% compared to the baseline. This indicates that a sufficient penalty weight is necessary to enforce distribution alignment, while the method remains robust across a reasonably wide range of α .
- The parameter C determines the margin of tolerated imbalance in the soft-margin relaxation. According to Table 6, strictly enforcing balance with smaller margins (e.g., $C = 0.001$) leads to significant improvements, such as a 2.3% MSE reduction on ETTh1. As C increases to 0.05, the constraints become overly relaxed, causing the performance to degrade towards the baseline (DF). This confirms that maintaining a tight bound on distribution discrepancy is crucial for effective model training.
- The integer K specifies the number of selected balancing functions based on their informativeness. Table 7 illustrates that even introducing a single balancing function ($K = 1$) provides a noticeable improvement over

Table 6. Varying C results.

| C | ETTh1 | | | | ETTm1 | | | |
|--------|-------|--------------|-------|--------------|-------|--------------|-------|--------------|
| | MSE | Δ MSE | MAE | Δ MAE | MSE | Δ MSE | MAE | Δ MAE |
| DF | 0.436 | - | 0.430 | - | 0.378 | - | 0.394 | - |
| 0.0005 | 0.431 | 1.2%↓ | 0.429 | 0.3%↓ | 0.374 | 1.0%↓ | 0.392 | 0.4%↓ |
| 0.001 | 0.426 | 2.3%↓ | 0.427 | 0.8%↓ | 0.374 | 1.0%↓ | 0.392 | 0.4%↓ |
| 0.005 | 0.431 | 1.2%↓ | 0.429 | 0.3%↓ | 0.373 | 1.3%↓ | 0.392 | 0.6%↓ |
| 0.01 | 0.430 | 1.3%↓ | 0.428 | 0.5%↓ | 0.373 | 1.3%↓ | 0.392 | 0.6%↓ |
| 0.05 | 0.434 | 0.5%↓ | 0.430 | 0.1%↓ | 0.374 | 1.0%↓ | 0.392 | 0.4%↓ |

Table 7. Varying K results.

| K | ETTh1 | | | | ETTm1 | | | |
|----|-------|--------------|-------|--------------|-------|--------------|-------|--------------|
| | MSE | Δ MSE | MAE | Δ MAE | MSE | Δ MSE | MAE | Δ MAE |
| DF | 0.436 | - | 0.430 | - | 0.378 | - | 0.394 | - |
| 1 | 0.432 | 0.8%↓ | 0.429 | 0.3%↓ | 0.374 | 1.1%↓ | 0.392 | 0.5%↓ |
| 2 | 0.431 | 1.1%↓ | 0.429 | 0.4%↓ | 0.374 | 1.1%↓ | 0.392 | 0.5%↓ |
| 3 | 0.427 | 2.1%↓ | 0.426 | 1.0%↓ | 0.374 | 1.1%↓ | 0.392 | 0.4%↓ |
| 4 | 0.432 | 0.8%↓ | 0.430 | 0.2%↓ | 0.374 | 0.9%↓ | 0.393 | 0.3%↓ |
| 5 | 0.427 | 2.1%↓ | 0.426 | 1.0%↓ | 0.374 | 1.1%↓ | 0.392 | 0.4%↓ |

the baseline. The performance gain peaks around $K = 3$ or $K = 4$, suggesting that a small set of the most discriminative kernels is sufficient to capture the primary distributional discrepancies. Further increasing K yields diminishing returns, validating the effectiveness of our selective balancing mechanism.

5. Conclusion

In this work, we identify a fundamental limitation in existing deep time-series forecasting objectives: they fail to satisfy Imbens’ criterion for true distribution balance, as they enforce moment matching only on a limited set of predefined functions. To address this, we propose Direct Forecasting with Kernelized Moment Balancing (KMB-DF) to ensure sufficient distribution alignment. Instead of relying on finite statistics, KMB-DF leverages Reproducing Kernel Hilbert Spaces (RKHS) to adaptively select infinite-dimensional balancing functions. We theoretically justify balancing joint distributions as a tractable proxy for aligning conditional distributions. Extensive experiments demonstrate that KMB-DF consistently achieves state-of-the-art performance by effectively mitigating autocorrelation bias.

Limitations. While KMB-DF enforces global statistical alignment via kernelized moment matching, it does not explicitly dictate sample-wise temporal correspondence. Consequently, KMB-DF functions optimally as a regularization term rather than a standalone objective. It requires a point-wise loss, such as MSE, to anchor element-wise alignment, allowing the framework to correct distributional discrepancies while maintaining temporal precision.

Impact Statement

This paper presents work whose goal is to advance the field of time-series forecasting. Improvements in forecasting ac-

curacy can yield substantial societal and economic benefits, including more reliable weather prediction, improved traffic management and scheduling, and more efficient planning and resource allocation in domains such as energy, logistics, and healthcare. The potential risks associated with improved time-series forecasting accuracy are less direct, none of which we feel must be specifically highlighted here.

References

Alkilane, K., He, Y., and Lee, D.-H. Mixmamba: Time series modeling with adaptive expertise. *Inf. Fusion*, 112: 102589, 2024.

Benidis, K., Rangapuram, S. S., Flunkert, V., Wang, Y., Mad-dix, D., Turkmen, C., Gasthaus, J., Bohlke-Schneider, M., Salinas, D., Stella, L., et al. Deep learning for time series forecasting: Tutorial and literature survey. *ACM Comput. Surv.*, 55(6):1–36, 2022.

Chen, H., Luong, V., Mukherjee, L., and Singh, V. Simpletm: A simple baseline for multivariate time series forecasting. In *Proc. Int. Conf. Learn. Represent.*, 2025.

Chen, Z., Ding, L., Chu, Z., Qi, Y., Huang, J., and Wang, H. Monotonic neural ordinary differential equation: Time-series forecasting for cumulative data. In *Proc. ACM Int. Conf. Inf. Knowl. Manag.*, pp. 4523–4529, 2023.

Cho, K., Van Merriënboer, B., Bahdanau, D., and Bengio, Y. On the properties of neural machine translation: Encoder-decoder approaches. *arXiv preprint arXiv:1409.1259*, 2014.

Cuturi, M. and Blondel, M. Soft-dtw: a differentiable loss function for time-series. In *Proc. Int. Conf. Mach. Learn.*, pp. 894–903. PMLR, 2017.

Das, A., Kong, W., Leach, A., Sen, R., and Yu, R. Long-term forecasting with tide: Time-series dense encoder. *Trans. Mach. Learn. Res.*, 2023.

Fong, C., Hazlett, C., and Imai, K. Covariate balancing propensity score for a continuous treatment: Application to the efficacy of political advertisements. *Ann. Appl. Stat.*, 12(1):156–177, 2018.

Gretton, A., Borgwardt, K. M., Rasch, M. J., Schölkopf, B., and Smola, A. A kernel two-sample test. *J. Mach. Learn. Res.*, 13(1):723–773, 2012.

Gu, A. and Dao, T. Mamba: Linear-time sequence modeling with selective state spaces. In *Proc. Conf. Lang. Model.*, 2023.

Hochreiter, S. and Schmidhuber, J. Long short-term memory. *Neural Comput.*, 9(8):1735–1780, 1997.

Hounie, I., Porras-Valenzuela, J., and Ribeiro, A. Loss shaping constraints for long-term time series forecasting. In *Proc. Int. Conf. Mach. Learn.*, 2024.

Imai, K. and Ratkovic, M. Covariate balancing propensity score. *J. R. Stat. Soc. Series. B. Stat. Methodol.*, 76(1): 243–263, 2014.

Imbens, G. W. and Rubin, D. B. *Causal inference in statistics, social, and biomedical sciences*. Cambridge University Press, 2015.

Jin, M., Wang, S., Ma, L., Chu, Z., Zhang, J. Y., Shi, X., Chen, P.-Y., Liang, Y., Li, Y.-F., Pan, S., et al. Time-lm: Time series forecasting by reprogramming large language models. *Proc. Int. Conf. Learn. Represent.*, 2024.

Kingma, D. P. and Ba, J. Adam: A method for stochastic optimization. In *Proc. Int. Conf. Learn. Represent.*, pp. 1–9, 2015.

Kong, Y., Wang, Z., Nie, Y., Zhou, T., Zohren, S., Liang, Y., Sun, P., and Wen, Q. Unlocking the power of lstm for long term time series forecasting. In *Proc. AAAI Conf. Artif. Intell.*, volume 39, pp. 11968–11976, 2025.

Kou, F., Wang, J., Shi, L., Yao, Y., Li, Y., Zhu, S., Zhang, Z., and Du, J. Cfpt: Empowering time series forecasting through cross-frequency interaction and periodic-aware timestamp modeling. In *Forty-second International Conference on Machine Learning*, 2025.

Kudrat, D., Xie, Z., Sun, Y., Jia, T., and Hu, Q. Patch-wise structural loss for time series forecasting. In *Proc. Int. Conf. Mach. Learn.*, 2025.

Lange, H., Brunton, S. L., and Kutz, J. N. From fourier to koopman: Spectral methods for long-term time series prediction. *Journal of Machine Learning Research*, 22(41):1–38, 2021.

Le Guen, V. and Thome, N. Shape and time distortion loss for training deep time series forecasting models. *Proc. Adv. Neural Inf. Process. Syst.*, 32, 2019.

Le Guen, V. and Thome, N. Deep time series forecasting with shape and temporal criteria. *IEEE Trans. Pattern Anal. Mach. Intell.*, 45(1):342–355, 2023.

Li, H., Xiao, Y., Zheng, C., Wu, P., and Cui, P. Propensity matters: Measuring and enhancing balancing for recommendation. In *Proc. Int. Conf. Mach. Learn.*, volume 202, pp. 20182–20194. PMLR, 2023.

Li, J., Liu, Y., Liu, W., Fang, S., Wang, L., Xu, C., and Bian, J. Mars: a financial market simulation engine powered by generative foundation model. In *Proc. Int. Conf. Learn. Represent.*, 2025.

Lin, S., Lin, W., Hu, X., Wu, W., Mo, R., and Zhong, H. Cyclenet: Enhancing time series forecasting through modeling periodic patterns. In *Proc. Adv. Neural Inf. Process. Syst.*, volume 37, pp. 106315–106345, 2024.

Lin, S., Chen, H., Wu, H., Qiu, C., and Lin, W. Temporal query network for efficient multivariate time series forecasting. In *Proc. Int. Conf. Mach. Learn.*, 2025.

Liu, B., Yuan, L., Shao, X., Wang, E., Xia, Z., Han, W., and Wu, C. Transformer-based generative adversarial network for traffic forecasting. *IEEE Trans. Consum. Electron.*, 2025.

Liu, P., Wu, B., Hu, Y., Li, N., Dai, T., Bao, J., and Xia, S.-t. Timebridge: Non-stationarity matters for long-term time series forecasting. *arXiv preprint arXiv:2410.04442*, 2024a.

Liu, X., Li, N., and Xia, S.-T. Gdtw: A novel differentiable dtw loss for time series tasks. In *Proc. IEEE Int. Conf. Acoust. Speech Signal Process.*, pp. 2860–2864. IEEE, 2021.

Liu, Y., Hu, T., Zhang, H., Wu, H., Wang, S., Ma, L., and Long, M. itransformer: Inverted transformers are effective for time series forecasting. In *Proc. Int. Conf. Learn. Represent.*, 2024b.

Liu, Y., Qin, G., Huang, X., Wang, J., and Long, M. Autotimes: Autoregressive time series forecasters via large language models. *Proc. Adv. Neural Inf. Process. Syst.*, 37:122154–122184, 2024c.

Luo, D. and Wang, X. Moderntcn: A modern pure convolution structure for general time series analysis. In *Proc. Int. Conf. Learn. Represent.*, pp. 1–43, 2024.

Makridakis, S., Spiliotis, E., and Assimakopoulos, V. M5 accuracy competition: Results, findings, and conclusions. *International journal of forecasting*, 38(4):1346–1364, 2022.

Mohri, M., Rostamizadeh, A., and Talwalkar, A. *Foundations of machine learning*. MIT press, 2018.

Nie, Y., Nguyen, N. H., Sinthong, P., and Kalagnanam, J. A time series is worth 64 words: Long-term forecasting with transformers. In *Proc. Int. Conf. Learn. Represent.*, 2023.

Piao, X., Chen, Z., Murayama, T., Matsubara, Y., and Sakurai, Y. Fredformer: Frequency debiased transformer for time series forecasting. In *Proc. ACM SIGKDD Int. Conf. Knowl. Discovery Data Mining*, pp. 2400–2410, 2024.

Qiu, X., Hu, J., Zhou, L., Wu, X., Du, J., Zhang, B., Guo, C., Zhou, A., Jensen, C. S., Sheng, Z., and Yang, B. Tfb: Towards comprehensive and fair benchmarking of time series forecasting methods. In *Proc. VLDB Endow.*, pp. 2363–2377, 2024.

Qiu, X., Wu, X., Cheng, H., Liu, X., Guo, C., Hu, J., and Yang, B. Dbloss: Decomposition-based loss function for time series forecasting. *Proc. Adv. Neural Inf. Process. Syst.*, 2025.

Rasul, K., Seward, C., Schuster, I., and Vollgraf, R. Autoregressive denoising diffusion models for multivariate probabilistic time series forecasting. In *Proc. Int. Conf. Mach. Learn.*, pp. 8857–8868. PMLR, 2021.

Sakoe, H. and Chiba, S. Dynamic programming algorithm optimization for spoken word recognition. *IEEE Trans. Signal Process.*, 26(1):43–49, 2003.

Salinas, D., Flunkert, V., Gasthaus, J., and Januschowski, T. Deepar: Probabilistic forecasting with autoregressive recurrent networks. *Int. J. Forecast.*, 36(3):1181–1191, 2020.

Tashiro, Y., Song, J., Song, Y., and Ermon, S. Csd: Conditional score-based diffusion models for probabilistic time series imputation. *Proc. Adv. Neural Inf. Process. Syst.*, 34:24804–24816, 2021.

Wang, H., Peng, J., Huang, F., Wang, J., Chen, J., and Xiao, Y. Micn: Multi-scale local and global context modeling for long-term series forecasting. In *Proc. Int. Conf. Learn. Represent.*, 2023.

Wang, H., Li, B., Fan, S., Wu, Y., and Liu, X. Timesql: Improving multivariate time series forecasting with multi-scale patching and smooth quadratic loss. *Inf. Sci.*, 671: 120652, 2024a.

Wang, H., Pan, L., Chen, Z., Chen, X., Dai, Q., Wang, L., Li, H., and Lin, Z. Time-o1: Time-series forecasting needs transformed label alignment. *Proc. Adv. Neural Inf. Process. Syst.*, 2025a.

Wang, H., Pan, L., Shen, Y., Chen, Z., Yang, D., Yang, Y., Zhang, S., Liu, X., Li, H., and Tao, D. Fredf: Learning to forecast in the frequency domain. In *Proc. Int. Conf. Learn. Represent.*, pp. 1–9, 2025b.

Wang, H., Pan, L., Lu, Y., Chen, Z., Liu, T., He, S., Chu, Z., Wen, Q., Li, H., and Lin, Z. Quadratic direct forecast for training multi-step time-series forecast models. In *Proc. Int. Conf. Learn. Represent.*, pp. 1–9, 2026a.

Wang, H., Pan, L., Lu, Y., Chu, Z., Li, X., He, S., Chen, Z., Li, H., Wen, Q., and Lin, Z. Distdf: Time-series forecasting needs joint-distribution wasserstein alignment. In *Proc. Int. Conf. Learn. Represent.*, pp. 1–9, 2026b.

Wang, Y., Wu, H., Dong, J., Liu, Y., Long, M., and Wang, J. Deep time series models: A comprehensive survey and benchmark. *arXiv preprint arXiv:2407.13278*, 2024b.

Wu, H., Xu, J., Wang, J., and Long, M. Autoformer: Decomposition transformers with Auto-Correlation for long-term series forecasting. In *Proc. Adv. Neural Inf. Process. Syst.*, 2021.

Wu, H., Hu, T., Liu, Y., Zhou, H., Wang, J., and Long, M. Timesnet: Temporal 2d-variation modeling for general time series analysis. In *Proc. Int. Conf. Learn. Represent.*, 2023a.

Wu, H., Zhou, H., Long, M., and Wang, J. Interpretable weather forecasting for worldwide stations with a unified deep model. *Nat. Mach. Intell.*, pp. 1–10, 2023b.

Wu, S., Xiao, X., Ding, Q., Zhao, P., Wei, Y., and Huang, J. Adversarial sparse transformer for time series forecasting. *Proc. Adv. Neural Inf. Process. Syst.*, 33:17105–17115, 2020.

Xiong, Q., Tang, K., Ma, M., Zhang, J., Xu, J., and Li, T. Modeling temporal dependencies within the target for long-term time series forecasting. *IEEE Trans. Knowl. Data Eng.*, 2025.

Yi, K., Zhang, Q., Fan, W., Wang, S., Wang, P., He, H., An, N., Lian, D., Cao, L., and Niu, Z. Frequency-domain mlps are more effective learners in time series forecasting. In *Proc. Adv. Neural Inf. Process. Syst.*, 2023.

Yue, W., Liu, Y., Li, H., Wang, H., Ying, X., Guo, R., Xing, B., and Shi, J. Olinear: A linear model for time series forecasting in orthogonally transformed domain. *Proc. Adv. Neural Inf. Process. Syst.*, 2025.

Zeng, A., Chen, M., Zhang, L., and Xu, Q. Are transformers effective for time series forecasting? In *Proc. AAAI Conf. Artif. Intell.*, 2023.

Zhou, H., Zhang, S., Peng, J., Zhang, S., Li, J., Xiong, H., and Zhang, W. Informer: Beyond efficient transformer for long sequence time-series forecasting. In *Proceedings of the AAAI conference on artificial intelligence*, volume 35, pp. 11106–11115, 2021.

Zhou, T., Ma, Z., Wen, Q., Wang, X., Sun, L., and Jin, R. FEDformer: Frequency enhanced decomposed transformer for long-term series forecasting. In *Proc. Int. Conf. Mach. Learn.*, 2022.

Zhou, T., Niu, P., Sun, L., Jin, R., et al. One fits all: Power general time series analysis by pretrained lm. *Proc. Adv. Neural Inf. Process. Syst.*, 36:43322–43355, 2023.

A. Extended Related Work

This section provides an extended review of deep time-series forecasting literature through the lens of autocorrelation modeling. As delineated in the Introduction, existing research primarily addresses two fundamental challenges: (1) devising neural architectures to model autocorrelation in history sequences, and (2) designing learning objectives to accommodate autocorrelation in label sequences.

A.1. Neural Architectures for History Autocorrelation

Recent advancements in neural architectures focus on capturing temporal dependencies within the historical input to generate latent representations for forecasting. These approaches can be broadly categorized into non-Transformer and Transformer-based models.

Non-Transformer Models. This category includes Recurrent Neural Networks (RNNs), Convolutional Neural Networks (CNNs), and Dense Neural Networks (DNNs). ① RNNs naturally model sequential autocorrelation via hidden states. While traditional RNNs (e.g., LSTM (Hochreiter & Schmidhuber, 1997), GRU (Cho et al., 2014)) suffer from efficiency bottlenecks, recent State Space Models (SSMs) like Mamba (Gu & Dao, 2023) and its variants (e.g., MixMamba (Alkilane et al., 2024)) have emerged to efficiently model long-range dependencies with linear complexity. ② CNNs capture local autocorrelation through convolutional kernels. To expand the receptive field for long-term forecasting, recent works employ large-kernel designs (e.g., ModernTCN (Luo & Wang, 2024)) or operate in the frequency domain (e.g., TimesNet (Wu et al., 2023a), MICN (Wang et al., 2023)). ③ DNNs utilizing simple linear layers have shown competitive performance by treating history sequences as feature vectors. Representative models like DLinear (Zeng et al., 2023) and TiDE (Das et al., 2023) demonstrate that Multi-Layer Perceptrons (MLPs) can effectively model autocorrelation when combined with decomposition or channel-independence strategies.

Transformer-based Models. Transformers utilize self-attention mechanisms to model high-order autocorrelation by computing pairwise similarities across time steps. ① Standard Self-Attention Models often employ tokenization to incorporate local context. For instance, PatchTST (Nie et al., 2023) segments series into patches to retain semantic meaning. A growing trend involves adapting Large Language Models (LLMs) for time-series (e.g., Time-LLM (Jin et al., 2024), GPT4TS (Zhou et al., 2023)) via reprogramming or fine-tuning to leverage their pre-trained reasoning capabilities. ② Modified Attention Models refine the attention mechanism to reduce complexity or enhance feature extraction. Notable approaches include frequency-domain attention (e.g., FedFormer (Zhou et al., 2022), FreDF (Wang et al., 2025b)) and inverted attention mechanisms that model correlations across variates (e.g., iTransformer (Liu et al., 2024b)).

A.2. Learning Objectives for Label Autocorrelation

While architectures focus on inputs, learning objectives aim to mitigate the bias arising from label autocorrelation, where future values are statistically dependent on their predecessors. Standard objectives like Mean Squared Error (MSE) assume conditional independence, leading to suboptimal training. Recent objectives mainly address this issue via likelihood estimation, shape alignment, conditional generation, and distribution balancing.

Likelihood Estimation. These methods aim to refine the negative log-likelihood (NLL) estimation. ① Label Transformation: To eliminate autocorrelation bias, methods like FreDF (Wang et al., 2025b) and Time-o1 (Wang et al., 2025a) transform labels into frequency or principal component domains, respectively, aiming to whiten the label distribution before applying point-wise losses. ② Covariance Modeling: Approaches such as QDF (Wang et al., 2026a) explicitly model the conditional covariance matrix to approximate the true NLL, often utilizing meta-learning or auxiliary networks.

Shape Alignment. Recognizing that autocorrelation manifests in morphological shapes, these objectives measure geometric dissimilarity. SoftDTW (Cuturi & Blondel, 2017) provides a differentiable relaxation of Dynamic Time Warping. Variants like Dilate (Le Guen & Thome, 2019) and STRIPE (Le Guen & Thome, 2023) further incorporate temporal distortion penalties to better align forecast shapes with ground truths.

Conditional Generation. This paradigm reframes forecasting as a generative task to implicitly capture label autocorrelation. Diffusion models (e.g., TimeGrad (Rasul et al., 2021), CSDI (Tashiro et al., 2021)) generate forecasts by learning the conditional distribution $\mathbb{P}(\mathbf{Y}|\mathbf{X})$ via iterative denoising. Autoregressive models (e.g., DeepAR (Salinas et al., 2020),

AutoTimes (Liu et al., 2024c)) generate predictions step-by-step to explicitly condition on previous outputs, though often suffering from error accumulation.

Distribution Balancing. Most relevant to our work, these methods view forecasting as aligning the distribution of forecasts with ground truths. ① Adversarial Training: Methods like AST (Wu et al., 2020) and variants (Liu et al., 2025) employ GAN-based discriminators to distinguish between predicted and real sequences, enforcing distributional alignment implicitly. ② Discrepancy Minimization: Recent works like DistDF (Wang et al., 2026b) explicitly minimize distributional discrepancies (e.g., joint-distribution Wasserstein distance).

While distribution balancing methods are theoretically appealing, existing approaches typically enforce moment matching only for limited or predefined functions (e.g., first/second moments in DistDF or specific discriminator architectures in AST). As discussed in Section 3.1, they fail to satisfy Imbens' criterion, which requires equivalence across **any** balancing function. Our proposed KMB-DF addresses this gap by leveraging the Reproducing Kernel Hilbert Space (RKHS) to adaptively select infinite dimensional balancing functions, ensuring sufficient distribution alignment.

B. Theoretical Justification

In this section, we delve into the theoretical underpinnings of the framework. By exploiting the universality, injectivity, and reproducing properties of kernel functions, we derive formal guarantees for the proposed method and demonstrate how these properties translate into effective balancing.

Lemma B.1 (Autocorrelation bias, Lemma 2.1 in the main text). *Let $\mathbf{y} \in \mathbb{R}^T$ be a univariate label sequence with conditional covariance $\Sigma \in \mathbb{R}^{T \times T}$. \mathcal{E}_{MSE} in (1) is biased against the likelihood of \mathbf{y} unless Σ is diagonal, i.e., different steps in \mathbf{y} are conditionally decorrelated given \mathbf{X} .*

Proof. The proof can be found in Theorem 3.1 of Wang et al. (2025a). \square

Lemma B.2 (Representer theorem). *Suppose $h(\|f\|) : \mathbb{R}_+ \rightarrow \mathbb{R}$ is a non-decreasing function. The minimizer of an empirical risk functional regularized by $h(\|f\|)$ admits the form: $f^*(\cdot) = \sum_{n=1}^N \alpha_n K(\cdot, \mathbf{Z}_n)$, where K is the kernel function associated with the RKHS \mathcal{H} .*

Proof. The proof can be found in Theorem 6.11 of Mohri et al. (2018). \square

Theorem B.3. *Suppose \mathcal{H} is the RKHS of a exponential kernel K , $f^* \in \mathcal{H}$ is the discrimination function that maximizes the discrepancy between two distributions \mathbb{P} and \mathbb{Q} . If f^* lies within the linear span of a finite kernel function set: $f^* \in \{K(\cdot, \mathbf{Z}_k)\}_{k=1}^K$; then \mathbb{P} and \mathbb{Q} are balanced if $\forall k \in [K] : \mathbb{E}_{\mathbf{Z} \sim \mathbb{P}}[K(\mathbf{Z}, \mathbf{Z}_k)] = \mathbb{E}_{\hat{\mathbf{Z}} \sim \mathbb{Q}}[K(\hat{\mathbf{Z}}, \mathbf{Z}_k)]$.*

Proof. We start by clarifying the maximum mean discrepancy (MMD) as our discrepancy measure between two distributions. Specifically, given a universal kernel K (e.g., exponential kernel), the MMD is defiend as:

$$\text{MMD}^2(\mathbb{P}, \mathbb{Q}) = \sup_{f \in \mathcal{H}, \|f\|_{\mathcal{H}} \leq 1} \left| \mathbb{E}_{\mathbf{Z} \sim \mathbb{P}}[f(\mathbf{Z})] - \mathbb{E}_{\hat{\mathbf{Z}} \sim \mathbb{Q}}[f(\hat{\mathbf{Z}})] \right|^2. \quad (9)$$

Let f^* be the discrimination function that maximizes the mean discrepancy between the two distributions \mathbb{P} and \mathbb{Q} , i.e., the function that achieves the supremum in the MMD² definition. By Lemma B.2, functions in \mathcal{H} can be represented as linear combinations of kernel functions. On the basis of this, by the assumption that f^* lies within the linear span of a finite kernel function set, there exist $\alpha_1, \dots, \alpha_K$ such that:

$$f^*(\cdot) = \sum_{k=1}^K \alpha_k K(\cdot, \mathbf{Z}_k). \quad (10)$$

Table 8. Dataset description.

| Dataset | D | Forecast length | Train / validation / test | Frequency | Domain |
|---------|-----|-------------------|---------------------------|-----------|-------------|
| ETTh1 | 7 | 96, 192, 336, 720 | 8545/2881/2881 | Hourly | Electricity |
| ETTh2 | 7 | 96, 192, 336, 720 | 8545/2881/2881 | Hourly | Electricity |
| ETTm1 | 7 | 96, 192, 336, 720 | 34465/11521/11521 | 15min | Electricity |
| ETTm2 | 7 | 96, 192, 336, 720 | 34465/11521/11521 | 15min | Electricity |
| ECL | 321 | 96, 192, 336, 720 | 18317/2633/5261 | Hourly | Electricity |
| Weather | 21 | 96, 192, 336, 720 | 36792/5271/10540 | 10min | Weather |
| M5 | 10 | 8, 12, 20, 28 | 1782/21/21 | Daily | Sale |

Note: D denotes the number of variates. $Frequency$ denotes the sampling interval of time points. $Train$, $Validation$, $Test$ denotes the number of samples employed in each split. The taxonomy aligns with (Wu et al., 2023a).

On this basis, we calculate the informativeness score where f^* serves as the balancing function:

$$\begin{aligned}
 \delta(f^*) &= \mathbb{E}_{\mathbf{Z} \sim \mathbb{P}}[f^*(\mathbf{Z})] - \mathbb{E}_{\hat{\mathbf{Z}} \sim \mathbb{Q}}[f^*(\hat{\mathbf{Z}})] \\
 &= \mathbb{E}_{\mathbf{Z} \sim \mathbb{P}} \left[\sum_{k=1}^K \alpha_k K(\mathbf{Z}, \mathbf{Z}_k) \right] - \mathbb{E}_{\hat{\mathbf{Z}} \sim \mathbb{Q}} \left[\sum_{k=1}^K \alpha_k K(\hat{\mathbf{Z}}, \mathbf{Z}_k) \right]. \\
 &\stackrel{(a)}{=} \sum_{k=1}^K \alpha_k \left(\mathbb{E}_{\mathbf{Z} \sim \mathbb{P}}[K(\mathbf{Z}, \mathbf{Z}_k)] - \mathbb{E}_{\hat{\mathbf{Z}} \sim \mathbb{Q}}[K(\hat{\mathbf{Z}}, \mathbf{Z}_k)] \right). \\
 &\stackrel{(b)}{=} 0
 \end{aligned} \tag{11}$$

where (a) exploits the linearity of the expectation operator to swap the summation and expectation; (b) applies the assumption that $\mathbb{E}_{\mathbf{Z} \in \mathbb{P}}[K(\mathbf{Z}, \mathbf{Z}_k)] = \mathbb{E}_{\hat{\mathbf{Z}} \in \mathbb{Q}}[K(\hat{\mathbf{Z}}, \mathbf{Z}_k)]$ for all $k = 1, \dots, K$.

Since f^* is the function that maximizes the mean discrepancy between \mathbb{P} and \mathbb{Q} , the maximum mean discrepancy is zero, *i.e.*, $\text{MMD}(\mathbb{P}, \mathbb{Q}) = 0$. Moreover, since K is a universal kernel, $\text{MMD}^2(\mathbb{P}, \mathbb{Q}) = 0$ implies $\mathbb{P} = \mathbb{Q}$ (Gretton et al., 2012), which completes the proof. \square

C. Reproduction Details

C.1. Dataset descriptions

Our empirical evaluation is conducted on a diverse collection of widely-used time series forecasting benchmarks. Each dataset presents distinct characteristics in terms of dimensionality and temporal resolution. A summary is provided in Table 8.

- **ETT** (Zhou et al., 2021): Contains seven metrics related to electricity transformers, recorded from July 2016 to July 2018. It is divided into four subsets based on sampling frequency: ETTh1 and ETTh2 (hourly), and ETTm1 and ETTm2 (every 15 minutes).
- **ECL** (Wu et al., 2021): Features the hourly electricity consumption of 321 clients.
- **Weather** (Wu et al., 2021): Comprises 21 meteorological variables from the Max Planck Biogeochemistry Institute's weather station, captured every 10 minutes throughout 2020.
- **M5** (Makridakis et al., 2022): Comprises 3049 individual products from 3 categories and 7 departments, sold in 10 stores in 3 states.

Following established protocols (Liu et al., 2024b; Qiu et al., 2024), all datasets are chronologically partitioned into training, validation, and test sets. For the ETT, Weather, and ECL, and datasets, we use a fixed history sequence length of 96 and

evaluate performance across four prediction horizons with lengths of 96, 192, 336, and 720. For the M5 datasets, we also use an historical length of 96 but evaluate on shorter prediction horizons of 8, 12, 20, and 28 steps. During the final evaluation on the test set, we ensure that no data is discarded from the last batch: a technique referred to as the *dropping-last trick* is disabled throughout our experiments.

C.2. Implementation details of model training

To ensure a rigorous and fair comparison, we strictly adhere to standard evaluation protocols established in recent literature (Liu et al., 2024b; Wu et al., 2023a). We reproduce all baseline methods using their official implementations, primarily integrating codes from the DistDF (Wang et al., 2026b) and CFPT (Kou et al., 2025) repositories. All models are optimized using the Adam optimizer (Kingma & Ba, 2015) with a fixed batch size of 32. Following Qiu et al. (2024), we disable the “drop-last” operation in data loaders during the testing phase to prevent data leakage and ensure metrics are calculated over the complete test set. To prevent overfitting, we employ an early stopping mechanism that terminates training if the validation loss fails to improve for 15 consecutive epochs. The initial learning rate is tuned for each dataset-model combination via a grid search over $\{5 \times 10^{-3}, 2 \times 10^{-3}, 10^{-3}, 5 \times 10^{-4}, 2 \times 10^{-4}, 10^{-4}, 5 \times 10^{-5}\}$, selecting the value that yields the minimal MSE on the validation set. All experiments are conducted on a computational cluster equipped with Intel(R) Xeon(R) Platinum 8463B CPUs and NVIDIA RTX H800 GPUs.

When integrating KMB-DF with forecast backbones (e.g., CFPT, TimeBridge), we explicitly retain the original models’ architectural hyperparameters as reported in their respective benchmarks to ensure that performance gains are attributed solely to the proposed objective. Consequently, our hyperparameter tuning is exclusively focused on the components of KMB-DF: the penalty strength α , the tolerated imbalance margin C , and the number of balancing functions K . Specifically, α is tuned within the interval $(0, 1]$ to balance the trade-off between the standard forecasting loss and the moment matching penalty. The margin C is selected from the set $\{0.0005, 0.001, 0.005, 0.01, 0.05\}$ to control the strictness of distribution alignment, while the number of balancing functions K is searched within the integer range $[1, 6]$. We utilize the exponential kernel as the default instantiation for the balancing functions.

D. More Experimental Results

D.1. Overall performance

Additional experimental results of overall performance are available in Table 9, where the performance given different T is reported.

D.2. Showcase

Additional experimental results of showcases are available in Figure 3, where two datasets are involved.

D.3. Generalization studies

Additional experimental results of varying forecast models are available in Figure 4, where four forecast models are involved on four datasets.

D.4. Case study with PatchTST of varying historical lengths

Additional experimental results of varying historical lengths are available in Table 10, complementing the fixed length of 96 used in the main text. The forecast models selected include CFPT (Kou et al., 2025) which is the recent state-of-the-art forecast model, and PatchTST (Nie et al., 2023) which is known to require large historical lengths. The results demonstrate that KMB-DF consistently improves both forecast models across different history sequence lengths.

D.5. Random Seed Sensitivity

Additional experimental results of random seed sensitivity are available in Table 11, where we report the mean and standard deviation of results obtained from experiments conducted with five different random seeds (2022, 2023, 2024, 2025, and 2026). The results indicate minimal sensitivity of the proposed method to random initialization, as most averaged standard deviations remain below 0.005.

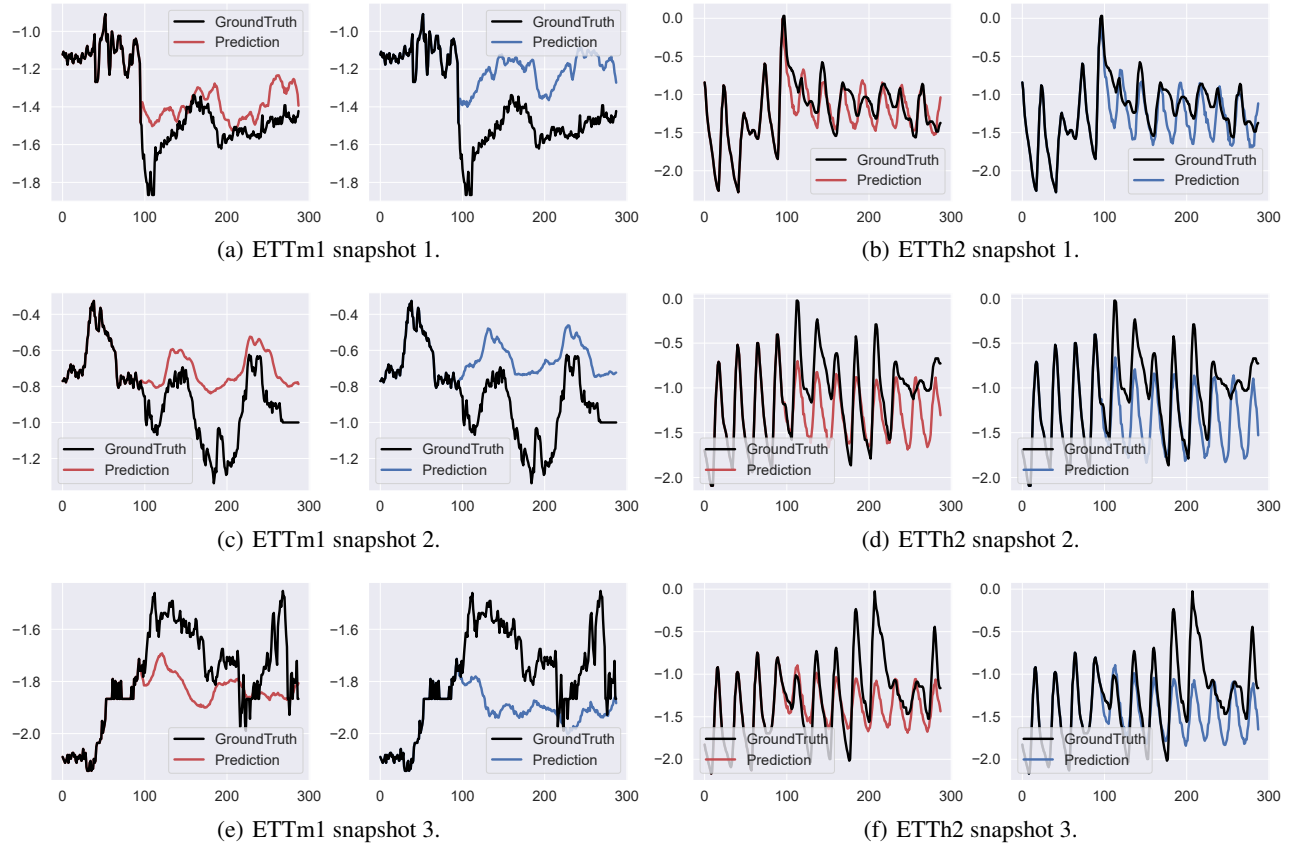


Figure 3. The forecast sequences generated with DF and KMB-DF. The forecast length is set to 192 and the experiment is conducted on ETTm1 and ETTh2.

Table 9. Full results on the multi-step forecasting task. The length of history window is set to 96 for all baselines. Avg indicates the results averaged over forecasting lengths: T=96, 192, 336 and 720 for ETT, ECL, and Weather; T=8, 12, 20 and 28 for M5.

| Loss | KMB-DF (Ours) | | QDF (2025) | | DistDF (2025) | | Time-o1 (2025) | | FreDF (2025) | | Koopman (2021) | | GDTW (2021) | | Dilate (2019) | | Soft-DTW (2017) | | MSE (2002) | |
|-----------------------|------------------|---------------------------|---------------------------|---------------------------|---------------------------|---------------------------|---------------------------|-------------|---------------------------|---------------------------|--------------------|-------------|----------------|-----|------------------|-----|--------------------|-----|---------------|-----|
| Metrics | MSE | MAE | MSE | MAE | MSE | MAE | MSE | MAE | MSE | MAE | MSE | MAE | MSE | MAE | MSE | MAE | MSE | MAE | MSE | MAE |
| ETTm1 | 96 | 0.315 0.352 | 0.318 0.359 | 0.318 0.355 | 0.321 0.353 | 0.320 0.354 | 0.326 0.363 | 0.324 0.362 | 0.323 0.361 | 0.322 0.359 | 0.321 0.358 | | | | | | | | | |
| | 192 | 0.351 0.379 | 0.355 0.379 | 0.356 0.380 | 0.358 0.380 | 0.356 0.379 | 0.359 0.383 | 0.368 0.392 | 0.363 0.385 | 0.366 0.385 | 0.357 0.382 | | | | | | | | | |
| | 336 | 0.381 0.400 | 0.384 0.401 | 0.383 0.401 | 0.386 0.403 | 0.386 0.401 | 0.383 0.401 | 0.405 0.421 | 0.384 0.401 | 0.399 0.409 | 0.387 0.401 | | | | | | | | | |
| | 720 | 0.442 0.433 | 0.443 0.435 | 0.444 0.434 | 0.447 0.436 | 0.444 0.434 | 0.446 0.436 | 0.496 0.473 | 0.446 0.437 | 0.490 0.461 | 0.446 0.435 | | | | | | | | | |
| | Avg | 0.372 0.391 | 0.375 0.393 | 0.375 0.393 | 0.378 0.393 | 0.376 0.392 | 0.378 0.395 | 0.398 0.412 | 0.379 0.396 | 0.394 0.403 | 0.378 0.394 | | | | | | | | | |
| ETTm2 | 96 | 0.166 0.249 | 0.168 0.250 | 0.168 0.251 | 0.173 0.251 | 0.174 0.251 | 0.182 0.262 | 0.176 0.257 | 0.172 0.253 | 0.176 0.256 | 0.175 0.256 | | | | | | | | | |
| | 192 | 0.229 0.291 | 0.232 0.292 | 0.232 0.293 | 0.233 0.291 | 0.233 0.290 | 0.235 0.294 | 0.243 0.305 | 0.236 0.296 | 0.243 0.299 | 0.234 0.295 | | | | | | | | | |
| | 336 | 0.289 0.330 | 0.288 0.329 | 0.289 0.330 | 0.290 0.329 | 0.290 0.327 | 0.291 0.331 | 0.303 0.344 | 0.290 0.331 | 0.306 0.342 | 0.289 0.330 | | | | | | | | | |
| | 720 | 0.384 0.388 | 0.386 0.387 | 0.385 0.387 | 0.386 0.385 | 0.386 0.386 | 0.388 0.390 | 0.434 0.419 | 0.393 0.390 | 0.438 0.422 | 0.385 0.389 | | | | | | | | | |
| | Avg | 0.267 0.315 | 0.268 0.315 | 0.269 0.315 | 0.271 0.314 | 0.271 0.313 | 0.274 0.319 | 0.289 0.332 | 0.273 0.317 | 0.291 0.330 | 0.271 0.317 | | | | | | | | | |
| ETTh1 | 96 | 0.372 0.389 | 0.373 0.392 | 0.373 0.391 | 0.369 0.392 | 0.373 0.389 | 0.374 0.393 | 0.377 0.395 | 0.376 0.394 | 0.377 0.394 | 0.373 0.391 | | | | | | | | | |
| | 192 | 0.423 0.420 | 0.426 0.421 | 0.426 0.420 | 0.424 0.424 | 0.424 0.418 | 0.426 0.424 | 0.434 0.427 | 0.430 0.423 | 0.436 0.427 | 0.427 0.421 | | | | | | | | | |
| | 336 | 0.460 0.438 | 0.464 0.441 | 0.468 0.441 | 0.464 0.439 | 0.465 0.439 | 0.466 0.440 | 0.486 0.457 | 0.470 0.442 | 0.479 0.451 | 0.466 0.441 | | | | | | | | | |
| | 720 | 0.447 0.455 | 0.473 0.464 | 0.467 0.462 | 0.462 0.460 | 0.472 0.468 | 0.483 0.469 | 0.512 0.497 | 0.489 0.478 | 0.551 0.510 | 0.477 0.468 | | | | | | | | | |
| | Avg | 0.426 0.426 | 0.434 0.429 | 0.434 0.428 | 0.430 0.429 | 0.434 0.428 | 0.437 0.431 | 0.452 0.444 | 0.441 0.434 | 0.461 0.445 | 0.436 0.430 | | | | | | | | | |
| ETTh2 | 96 | 0.285 0.337 | 0.288 0.337 | 0.287 0.337 | 0.286 0.336 | 0.289 0.337 | 0.287 0.338 | 0.289 0.340 | 0.287 0.338 | 0.292 0.342 | 0.287 0.337 | | | | | | | | | |
| | 192 | 0.363 0.387 | 0.367 0.390 | 0.364 0.391 | 0.367 0.384 | 0.365 0.382 | 0.365 0.390 | 0.377 0.399 | 0.368 0.389 | 0.380 0.398 | 0.368 0.390 | | | | | | | | | |
| | 336 | 0.411 0.425 | 0.412 0.427 | 0.412 0.426 | 0.414 0.427 | 0.414 0.427 | 0.413 0.429 | 0.422 0.432 | 0.413 0.427 | 0.455 0.443 | 0.416 0.428 | | | | | | | | | |
| | 720 | 0.396 0.426 | 0.401 0.428 | 0.398 0.427 | 0.402 0.428 | 0.406 0.430 | 0.405 0.430 | 0.457 0.463 | 0.415 0.437 | 0.445 0.453 | 0.415 0.436 | | | | | | | | | |
| | Avg | 0.364 0.394 | 0.367 0.396 | 0.365 0.395 | 0.367 0.394 | 0.368 0.394 | 0.368 0.397 | 0.386 0.409 | 0.371 0.398 | 0.393 0.409 | 0.372 0.398 | | | | | | | | | |
| ECL | 96 | 0.136 0.231 | 0.137 0.232 | 0.137 0.232 | 0.141 0.235 | 0.139 0.232 | 0.138 0.232 | 0.882 0.777 | 0.137 0.232 | 0.136 0.232 | 0.137 0.232 | | | | | | | | | |
| | 192 | 0.152 0.245 | 0.153 0.246 | 0.152 0.246 | 0.154 0.246 | 0.156 0.246 | 0.153 0.247 | 0.853 0.762 | 0.154 0.247 | 0.154 0.247 | 0.153 0.247 | | | | | | | | | |
| | 336 | 0.168 0.265 | 0.168 0.264 | 0.168 0.265 | 0.168 0.263 | 0.169 0.263 | 0.169 0.267 | 0.809 0.711 | 0.169 0.267 | 0.169 0.267 | 0.168 0.266 | | | | | | | | | |
| | 720 | 0.198 0.293 | 0.199 0.293 | 0.201 0.294 | 0.198 0.291 | 0.199 0.290 | 0.201 0.296 | 0.900 0.769 | 0.202 0.297 | 0.203 0.298 | 0.199 0.294 | | | | | | | | | |
| | Avg | 0.163 0.258 | 0.164 0.259 | 0.164 0.259 | 0.165 0.259 | 0.166 0.258 | 0.165 0.260 | 0.861 0.755 | 0.165 0.260 | 0.165 0.261 | 0.165 0.260 | | | | | | | | | |
| Weather | 96 | 0.152 0.196 | 0.155 0.200 | 0.155 0.200 | 0.153 0.197 | 0.154 0.197 | 0.173 0.215 | 0.158 0.206 | 0.173 0.215 | 0.177 0.220 | 0.156 0.201 | | | | | | | | | |
| | 192 | 0.204 0.242 | 0.205 0.244 | 0.205 0.245 | 0.205 0.243 | 0.204 0.242 | 0.205 0.245 | 0.209 0.250 | 0.205 0.246 | 0.209 0.245 | 0.205 0.245 | | | | | | | | | |
| | 336 | 0.260 0.284 | 0.261 0.285 | 0.261 0.286 | 0.261 0.284 | 0.261 0.284 | 0.284 0.288 | 0.262 0.286 | 0.270 0.296 | 0.262 0.287 | 0.278 0.296 | 0.261 0.286 | | | | | | | | |
| | 720 | 0.339 0.337 | 0.343 0.338 | 0.343 0.341 | 0.343 0.340 | 0.341 0.338 | 0.345 0.342 | 0.354 0.352 | 0.345 0.342 | 0.385 0.363 | 0.343 0.339 | | | | | | | | | |
| | Avg | 0.239 0.265 | 0.241 0.267 | 0.241 0.268 | 0.240 0.266 | 0.240 0.265 | 0.246 0.272 | 0.248 0.276 | 0.246 0.273 | 0.262 0.281 | 0.241 0.267 | | | | | | | | | |
| M5 | 8 | 0.150 0.307 | 0.152 0.309 | 0.152 0.308 | 0.159 0.318 | 0.151 0.308 | 0.154 0.311 | 0.153 0.312 | 0.154 0.312 | 0.154 0.312 | 0.151 0.309 | | | | | | | | | |
| | 12 | 0.151 0.311 | 0.152 0.311 | 0.154 0.311 | 0.164 0.325 | 0.155 0.313 | 0.156 0.314 | 0.160 0.319 | 0.161 0.319 | 0.160 0.319 | 0.157 0.315 | | | | | | | | | |
| | 20 | 0.153 0.311 | 0.155 0.313 | 0.154 0.313 | 0.159 0.317 | 0.166 0.328 | 0.158 0.318 | 0.163 0.321 | 0.165 0.326 | 0.164 0.326 | 0.165 0.324 | | | | | | | | | |
| | 28 | 0.154 0.309 | 0.165 0.320 | 0.162 0.322 | 0.162 0.316 | 0.199 0.361 | 0.164 0.323 | 0.164 0.319 | 0.156 0.311 | 0.169 0.332 | 0.169 0.331 | 0.199 0.361 | | | | | | | | |
| | Avg | 0.152 0.309 | 0.156 0.313 | 0.156 0.313 | 0.161 0.319 | 0.168 0.327 | 0.158 0.317 | 0.160 0.318 | 0.159 0.317 | 0.162 0.322 | 0.168 0.327 | | | | | | | | | |
| 1 st Count | 33 | 24 | 1 | 0 | 0 | 0 | 1 | 2 | 0 | 9 | 0 | 0 | 0 | 0 | 0 | 0 | 0 | 0 | 0 | 0 |

D.6. Complexity Analysis

We empirically evaluate the computational overhead of KMB-DF, as illustrated in Figure 5. The experiments are conducted with a batch size of 128, variable dimension $D = 21$, and the number of balancing functions $K = 3$. As the forecast horizon T extends from 32 to 720, the running time for both forward and backward passes exhibits a marginal upward trend. This is expected, as a larger T increases the length of the joint sequences Z , thereby slightly scaling the kernel matrix calculations required for moment balancing. However, the absolute overhead remains negligible; even at the longest horizon of $T = 720$, the forward pass takes less than 0.73 ms, and the backward pass requires approximately 0.31 ms. Crucially, these additional computations are exclusive to the training phase. During inference, the KMB-DF objective is removed, ensuring that the model's inference speed is unaffected. Consequently, KMB-DF enhances forecasting performance with minimal training cost and *zero* additional inference latency.

Table 10. Varying input sequence length results on the Weather dataset.

| Models | | KMB-DF | | | | CFPT | | KMB-DF | | PatchTST | |
|----------------------------|-----|---------|--|-------|-------|-------|-------|--------|-------|----------|-------|
| | | Metrics | | MSE | MAE | MSE | MAE | MSE | MAE | MSE | MAE |
| Historical sequence length | 96 | 96 | | 0.152 | 0.196 | 0.156 | 0.201 | 0.178 | 0.219 | 0.189 | 0.230 |
| | | 192 | | 0.204 | 0.242 | 0.205 | 0.245 | 0.224 | 0.259 | 0.228 | 0.262 |
| | | 336 | | 0.260 | 0.284 | 0.261 | 0.286 | 0.280 | 0.299 | 0.288 | 0.305 |
| | | 720 | | 0.339 | 0.337 | 0.343 | 0.339 | 0.356 | 0.348 | 0.362 | 0.354 |
| | | Avg | | 0.239 | 0.265 | 0.241 | 0.267 | 0.260 | 0.281 | 0.267 | 0.288 |
| | 192 | 96 | | 0.148 | 0.196 | 0.150 | 0.198 | 0.159 | 0.204 | 0.163 | 0.209 |
| | | 192 | | 0.193 | 0.238 | 0.195 | 0.239 | 0.206 | 0.247 | 0.207 | 0.249 |
| | | 336 | | 0.247 | 0.278 | 0.250 | 0.282 | 0.260 | 0.289 | 0.268 | 0.293 |
| | | 720 | | 0.325 | 0.331 | 0.330 | 0.333 | 0.335 | 0.339 | 0.338 | 0.339 |
| | | Avg | | 0.228 | 0.261 | 0.231 | 0.263 | 0.240 | 0.270 | 0.244 | 0.273 |
| | 336 | 96 | | 0.143 | 0.192 | 0.145 | 0.195 | 0.153 | 0.202 | 0.158 | 0.208 |
| | | 192 | | 0.188 | 0.235 | 0.188 | 0.235 | 0.195 | 0.242 | 0.235 | 0.291 |
| | | 336 | | 0.240 | 0.275 | 0.240 | 0.277 | 0.249 | 0.283 | 0.252 | 0.287 |
| | | 720 | | 0.317 | 0.328 | 0.321 | 0.332 | 0.323 | 0.337 | 0.326 | 0.336 |
| | | Avg | | 0.222 | 0.258 | 0.224 | 0.260 | 0.230 | 0.266 | 0.243 | 0.280 |
| | 720 | 96 | | 0.144 | 0.196 | 0.148 | 0.200 | 0.150 | 0.201 | 0.153 | 0.205 |
| | | 192 | | 0.190 | 0.239 | 0.189 | 0.240 | 0.196 | 0.245 | 0.205 | 0.254 |
| | | 336 | | 0.239 | 0.279 | 0.238 | 0.279 | 0.244 | 0.285 | 0.248 | 0.288 |
| | | 720 | | 0.307 | 0.327 | 0.310 | 0.329 | 0.313 | 0.335 | 0.317 | 0.339 |
| | | Avg | | 0.220 | 0.260 | 0.221 | 0.262 | 0.226 | 0.266 | 0.231 | 0.272 |

 Table 11. Experimental results (mean \pm std) with varying seeds (2022-2026).

| Dataset | ETTh1 | | | | | | | | ETTm1 | | | | | | | |
|---------|-------------------|-------------------|-------------------|-------------------|-------------------|-------------------|-------------------|-------------------|--------|-----|-----|-----|-----|-----|-----|-----|
| | KMB-DF | | | | DF | | | | KMB-DF | | | | DF | | | |
| Metrics | MSE | MAE | MSE | MAE | MSE | MAE | MSE | MAE | MSE | MAE | MSE | MAE | MSE | MAE | MSE | MAE |
| 96 | 0.372 \pm 0.002 | 0.390 \pm 0.001 | 0.373 \pm 0.000 | 0.391 \pm 0.000 | 0.320 \pm 0.004 | 0.356 \pm 0.003 | 0.319 \pm 0.004 | 0.357 \pm 0.002 | | | | | | | | |
| 192 | 0.425 \pm 0.001 | 0.421 \pm 0.001 | 0.427 \pm 0.000 | 0.421 \pm 0.000 | 0.354 \pm 0.002 | 0.380 \pm 0.001 | 0.359 \pm 0.005 | 0.382 \pm 0.001 | | | | | | | | |
| 336 | 0.459 \pm 0.001 | 0.437 \pm 0.001 | 0.468 \pm 0.002 | 0.442 \pm 0.001 | 0.385 \pm 0.002 | 0.402 \pm 0.001 | 0.390 \pm 0.002 | 0.402 \pm 0.001 | | | | | | | | |
| 720 | 0.462 \pm 0.013 | 0.463 \pm 0.006 | 0.475 \pm 0.003 | 0.467 \pm 0.002 | 0.443 \pm 0.001 | 0.434 \pm 0.000 | 0.446 \pm 0.000 | 0.435 \pm 0.000 | | | | | | | | |
| Avg | 0.429 \pm 0.004 | 0.428 \pm 0.002 | 0.436 \pm 0.001 | 0.430 \pm 0.001 | 0.375 \pm 0.002 | 0.393 \pm 0.001 | 0.379 \pm 0.002 | 0.394 \pm 0.001 | | | | | | | | |

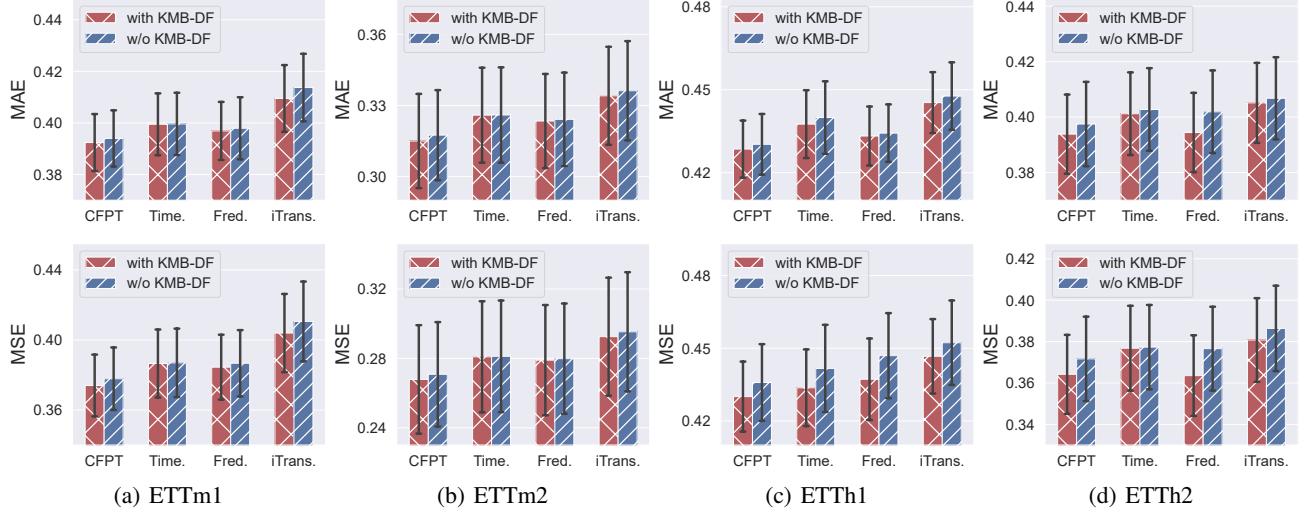


Figure 4. Performance of different forecast models with and without KMB-DF. The forecast errors are averaged over forecast lengths and the error bars represent 50% confidence intervals.

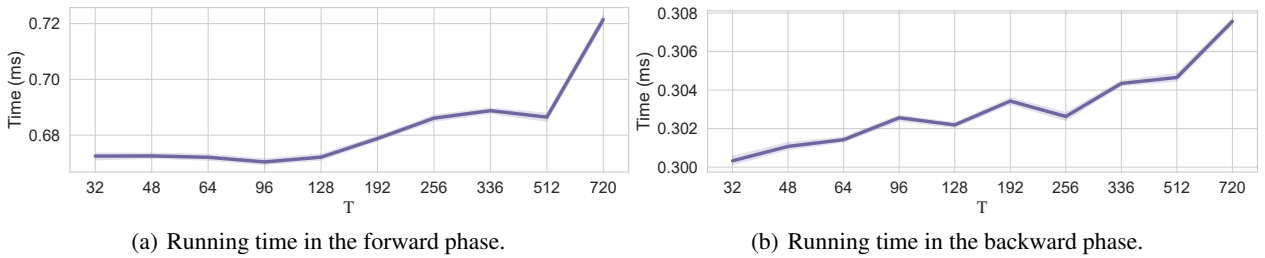


Figure 5. Running time (ms) with varying forecast horizons.